

# THE DWARF GALAXY POPULATION IN NEARBY GROUPS. THE DATA<sup>1</sup>

ELEAZAR R. CARRASCO<sup>2</sup>

Gemini Observatory, Southern Operations Center, AURA, Casilla 603, La Serena, Chile; rcarrasco@gemini.edu

CLAUDIA MENDES DE OLIVEIRA

Instituto de Astronomia, Geofísica e Ciências Atmosféricas, Departamento de Astronomia, Universidade de São Paulo, Rua do Matão 1226, Cidade Universitária, 05508-900, SP, Brazil; oliveira@astro.iag.usp.br

AND

LEOPOLDO INFANTE

Departamento de Astronomía y Astrofísica, Pontificia Universidad Católica de Chile, Vicuña Mackenna 4860, Casilla 306, Santiago 22, Chile; linfante@astro.puc.cl

*Revised version. Submitted 2006 May 22*

## ABSTRACT

We used  $V$  and  $I$  CCD photometry to search for low-surface brightness dwarf galaxies in the central ( $< 0.5 \text{ h}^{-1} \text{ Mpc}$ ) region of the loose groups NGC 6868 (Telescopium) and NGC 5846, the compact group HCG 42 and the poor cluster IC 4765. We used the parameters given by the exponential profile fit (central surface brightness, scale length and limiting diameter) to identify 80 low surface-brightness dwarf candidates with magnitudes  $17 < V < 22 \text{ mag}$  ( $-16.7 > M_V > -11.4$  at the assumed distances of the groups) and with colors  $V - I < 1.5 \text{ mag}$  at the limiting isophote of  $25.8 \text{ V mag/arcsec}^2$ . The selected galaxies have central surface brightnesses  $\mu_0 > 22.5 \text{ V mag/arcsec}^2$ , scale lengths  $h > 1.5''$ , and diameters larger than  $1.2 \text{ h}^{-1} \text{ kpc}$ . Twenty of the eighty galaxies are extended low surface-brightness galaxies that were detected only on smoothed images, after masking all high surface brightness objects. The completeness fraction in the detection of the low surface-brightness dwarf galaxies is  $\sim 80\%$  for  $V \lesssim 20$  and  $22.5 < \mu_0 < 24.5 \text{ V mag/arcsec}^2$ , and below  $50\%$  at fainter magnitudes and central surface brightnesses ( $\mu_0 > 24.5 \text{ V mag/arcsec}^2$  and  $V > 20 \text{ mag}$ ). In this last bin, the completeness increases to  $\sim 80\%$  when we search for galaxies in smoothed images instead.

The detected low surface-brightness dwarf galaxies are highly concentrated towards the center of the four groups in the inner  $250 \text{ h}^{-1} \text{ kpc}$ . At larger radii, the projected number density is similar to the value found in the control fields. The best fit power-law slope of the surface density distribution is, on average,  $\beta \sim -1.5$  ( $R < 250 \text{ h}^{-1} \text{ kpc}$ ), in agreement with the values found for satellites dwarfs around isolated E/S0 galaxies and in X-ray groups. The distribution of the low surface-brightness dwarf galaxies in the  $M_V - \mu_0$  plane does not show a clear correlation, suggesting that the correlation noted by other studies could be produced by selection effects. The low surface-brightness dwarf galaxies follow a well defined color-magnitude relation, extending for more than ten magnitudes (from bright ellipticals to faint dwarfs). A similar well defined color-magnitude relation from giants to dwarfs is known to be valid for galaxy clusters but it is the first time that it is demonstrated in the sparse environments of groups.

The spectroscopic follow-up shows that only 78 of the 412 galaxies with measured velocities in the fields of these groups are group members. We were able to obtain the radial velocity for 11 of the 80 low-surface brightness dwarf galaxies. Five of these galaxies are group members while six are in the background of the groups. We infer, then, that more than  $90\%$  of the 80 low surface-brightness dwarf galaxies in our sample must be bonafide group members. In addition, new structures along the group's lines-of-sights were discovered. These new structures are groups and poor clusters that extend to  $\sim 0.3$  in redshift space.

*Subject headings:* galaxies: clusters: general – galaxies: photometry – galaxies: fundamental parameters (classification, colors, surface brightness) – galaxies: dwarfs: – galaxies: cluster: individual (HCG 42, IC 4765, NGC 5846, NGC 6868)

## 1. INTRODUCTION

Groups are the most common environment of galaxies in the Universe. Most galaxies are associated to these poor systems and, due to their low velocity dispersions,

these systems are good laboratories to study the different physical processes that regulate galaxy formation and evolution.

Nearby galaxy groups are characterized by their small numbers of bright galaxies (typically 5–7 galaxies brighter than  $M^*$ ). Usually redshifts are known only for the brightest members, and no redshift information is available for the galaxies at fainter magnitudes.

The faint-end of the luminosity distribution is the

<sup>1</sup> Based upon data collected on the 1.3m Warsaw telescope and 2.5m Du Pont telescope at Las Campanas Observatory, Chile

<sup>2</sup> Visiting Astronomer, Las Campanas Observatory. Las Campanas Observatory is operated by the Carnegie Institution of Washington.

regime where the dwarf galaxies dominate. Dwarf galaxies are exceptional laboratories for the study of many physical processes, such as structure formation, galaxy evolution, star formation, and dark matter distribution. However, the low luminosity and surface brightness of these objects have limited most of the previous studies done so far. Because of their low-luminosities, spectroscopic observations of these objects are extremely difficult and time consuming. Except for the Local Group and other nearby structures (e.g. M81, Sculptor, LeoI, ComaI: Jerjen, Freeman & Binggeli 1998; Jerjen, Binggeli & Freeman 2000; Trentham & Tully 2002; Bremnes et al. 1998; Flint et al. 2001, 1999) the physical characterization of dwarf galaxies and its implication to galaxy formation and evolution is poorly constrained. In the last few years, the advent of a new generation of telescopes and new large-format CCD detectors opened a unique possibility to search and detect the low surface-brightness dwarf galaxy population of nearby systems. It became possible to obtain deep photometry for statistically significant samples of these galaxies in large areas of nearby groups and clusters (e.g. Carrasco et al. 2001; Trentham & Tully 2002; Trentham, Sampson & Banerji 2005).

This is the second paper of a series dedicated to survey nearby groups with the aim of identifying the population of low surface brightness dwarf galaxies (LSBD) down to  $M_V = -13$  mag. The main goal is to identify the LSBD and to characterize and study the physical properties and the Galaxy Luminosity Function of the groups (the latter will be presented in a later paper). The program started with the observation of the Dorado group at  $cz \sim 1200$  km s $^{-1}$  (Carrasco et al. 2001) and continued with the observation of other four nearby groups with  $1000 < cz < 4500$  km s $^{-1}$ , described here. In this paper we present the results of the photometric and spectroscopic study of the galaxy population in NGC 6868, NGC 5846, HCG 42 and IC 4765.

The paper is organized as follows. In Section 2 we describe the sample. The observations, the data reduction and the estimation of the photometric errors and completeness of the spectroscopic sample is presented in section 3. In section 4 we explain the criteria used to select the LSBD sample, the determination of the completeness fractions in the detection of Local Group-like dwarf galaxies at the distance of the groups, and the photometric analysis of the LSBD galaxies detected. Section 5 is devoted to analyse the spectroscopic survey, while in section 6 we present the main results. Finally, our conclusions are presented in Section 7.

For all calculations, the following cosmological parameters were assumed:  $\Omega_M = 0.2$ ,  $\Omega_\Lambda = 0.8$  with a Hubble constant of  $H_0 = 75$  km s $^{-1}$  Mpc $^{-1}$ . Here  $h$  is a dimensionless constant defined as the Hubble constant divided by 75 km s $^{-1}$  Mpc $^{-1}$ , i.e.  $h = H/75$ .

## 2. THE SAMPLE

The four groups studied were selected from the catalog of Garcia (1993). The groups vary in richness and density, with galaxy populations which differ widely in morphological fractions. Some of their characteristics are described below.

The Hickson Compact Group 42 (HCG 42; Hickson 1982) is dominated by the giant elliptical galaxy

NGC3091 (E3) and by the galaxies HCG 42b (SB0), HCG 42c (E2) and HCG 42d (E2). The group has a galaxy density of  $\sim 25$  gal/deg $^2$  inside a radius of 0.3 h $^{-1}$  Mpc an brighter than  $M_V \sim -18$  mag (Zabludoff & Mulchaey 1998) with a high number of faint galaxies superimposed onto the region. In fact, Rood & Struble (1994) found evidence that this system could be associated to the poor group NGC 3091 (or LGG186; Garcia 1993), suggesting that HCG 42 is an intermediate structure: a compact group inside a more extended system (de Carvalho, Ribeiro & Zepf 1994). X-ray maps from the ROSAT satellite analyzed by Ebeling, Voges & Böhringer (1994) showed that this group has an extended X-ray emission. Further analysis by Ponman et al. (1996) and Mulchaey & Zabludoff (1998) showed that HCG 42 has two components in the gas emission, one centered around NGC 3091 galaxy, with  $L_X \sim 10^{41}$  h $^{-2}$  erg s $^{-1}$  and a second, more extended, that could be associated to the global potential well of the group (Mulchaey & Zabludoff 1998; Mulchaey et al. 2003). The assumed distance to HCG 42, shown in Table 1 (col 1), is based on the distance to the galaxy NGC 3091, obtained by the  $D_n - \sigma$  method (Faber et al. 1989).

The NGC 5846 group (GH150;LGG929 Geller & Huchra 1983; Garcia 1993) is dominated by the giant elliptical galaxy of the same name (E0) and by the galaxies NGC 5846A (cE2), NGC 5850 (SB(r)b), NGC 5845 (E1) and NGC 5839 (SAB(r)). For galaxies  $M_V \sim -18$  mag, the group has a density of  $\sim 11$  gal/deg $^2$  inside a radius of 0.3 h $^{-1}$  Mpc (Zabludoff & Mulchaey 1998). This group is part of an extended cloud of galaxies detected in the Virgo-Libra direction. Also, it shows an extended X-ray emission, with two clear components, one, with a luminosity  $L_X \sim 10^{41}$  h $^{-2}$  erg s $^{-1}$  centered on NGC 5846 and a second, more extended, with  $L_X \sim 10^{42}$  h $^{-2}$  erg s $^{-1}$  (Mulchaey & Zabludoff 1998; Mulchaey et al. 2003) associated to the intragroup medium. The assumed distance to this group (see Table 1) is based on the average distance to the five brightest galaxies, determined through the surface brightness fluctuation method (Tonry et al 2000).

IC 4765 (Sersic 129-01, PavoII, DC1842-63, Abell S805, LGG422; Sérsic 1974; Dressler 1980; Abell, Corwin & Olowin 1989; Garcia 1993) is defined as a poor cluster of galaxies (Bautz-Morgan I, richness 0). However, it could also be treated as a rich group. It is located close to the galactic plane ( $b \sim -23$  deg) and it is dominated by the D galaxy IC 4765 and by a barred spiral galaxy IC 4749 (SB(rs)bc and 11 arcmin south of IC 4765). Following Quintana & Melnick (1975), this group is formed by two structures in interaction: one poor, spiral rich, centered around IC 4749 and another rich sub-system centered around IC 4765. The group shows X-ray emission  $L_X = 3.6 \times 10^{43}$  h $^{-2}$  erg s $^{-1}$  (Jones & Forman 1999) and a moderate *cooling flow* (White, Jones & Forman 1997). There is no information in the literature about the distance to this cluster. The value in Table 1 has been calculated assuming that the redshift is a good indicator of the distance.

The last studied group, NGC 6868 (Telescopium, LGG430; Garcia 1993), extends for more than 2 degrees on the sky and shows an elongated form in the East-West direction. It is dominated by the giant elliptical galaxy NGC 6868 (E2) and by the galaxies ESO233-G035

(S0), NGC6870 (SAB(rs)ab) and NGC 6861D (SA(s)). The group shows a low X-ray emission with  $L_X \sim 10^{41} \text{ h}^{-2} \text{ erg s}^{-1}$  centered on NGC 6868 galaxy (Beuing et al. 1999). Garcia (1993) identified 11 galaxies brighter than  $M_V = -18$  as group members, while Ramella et al. (1996) identified five other members. The assumed distance to this group is based on the average distance to the five brightest group galaxies determined through the Surface brightness fluctuation method (Tonry et al 2000).

The group parameters shown in Table 1 are (1) group name; (2) and (3) the equatorial coordinates; (4) the distance; (5) velocity dispersion; (6) bolometric X-ray luminosity; (7) and (8) the interstellar extinctions in the direction of the groups. Extinction values have been obtained from the maps of Schlegel et al. (1998) using the relations  $A_V = 3.1 \times E(B-V)$  and  $A_I = 1.5 \times E(B-V)$  from Cardelli et al. (1989).

### 3. OBSERVATION AND DATA REDUCTION

#### 3.1. Imaging

The groups were observed in February and March 1998, with the 1.3m Warsaw telescope (Udalsky et al. 1997) located in Las Campanas Observatory, Chile, using the SIT1 2048  $\times$  2048 CCD detector. With a pixel size of  $24\mu\text{m}$  and a scale of  $0.414''/\text{pix}$ , the detector covers an area of  $14.13 \times 14.13 \text{ arcmin}^2$  on the sky.

The groups were imaged through the standard Johnson V and Cousins I filters. All observations were done under photometric conditions, except for one of the fields in NGC 6868. For this field, a calibration image observed under photometric conditions and in a different night, was obtained in order to derived the correct zero-point. The seeing conditions were relatively good and varied between  $1.2''$  and  $1.5''$  in both filters. The derived seeing values per filter for each of the observed fields are tabulated in Table 1 (see below).

We have observed each group with several different pointings, covering the central area, following a mosaic pattern. The total areas observed in the central region of the group were: for HCG 42,  $28 \times 28 \text{ arcmin}^2$  (5 fields); for NGC 5846,  $42 \times 14 \text{ arcmin}^2$  (3 fields); for IC 4765,  $14 \times 28 \text{ arcmin}^2$  (2 fields); and for NGC 6868,  $28 \times 14 \text{ arcmin}^2$  (2 fields). These values correspond to a physical area of  $\sim 0.44 \times 0.44 \text{ h}^{-2} \text{ Mpc}^2$ ,  $0.29 \times 0.10 \text{ h}^{-2} \text{ Mpc}^2$ ,  $\sim 0.24 \times 0.48 \text{ h}^{-2} \text{ Mpc}^2$  and  $\sim 0.26 \times 0.13 \text{ h}^{-2} \text{ Mpc}^2$  at the distance of HCG 42, NGC 5846, IC 4665 and NGC 6868 respectively. For three of the groups (all but NGC 6868), observations of control fields in both filters were obtained in order to estimate the background and foreground galaxy counts (9 fields). We pointed the telescope 2-3 deg from the center of the groups to acquire these control fields.

All frames were observed with a small overlap between them ( $\sim 20 - 30 \text{ arcsec}$ ) in order to check the photometry and estimate the photometric errors. The details of the observations are contained in Table 2. The table shows the number of fields observed in each group (column 2), the field positions (columns 3 and 4), the filters used and the total exposure time per filter (columns 5, 6 and 7), the derived seeing per filter (columns 8 and 9) and the total area covered in each group. The projected distribution of all observed fields is shown in Fig. 1. We also included in the figure all

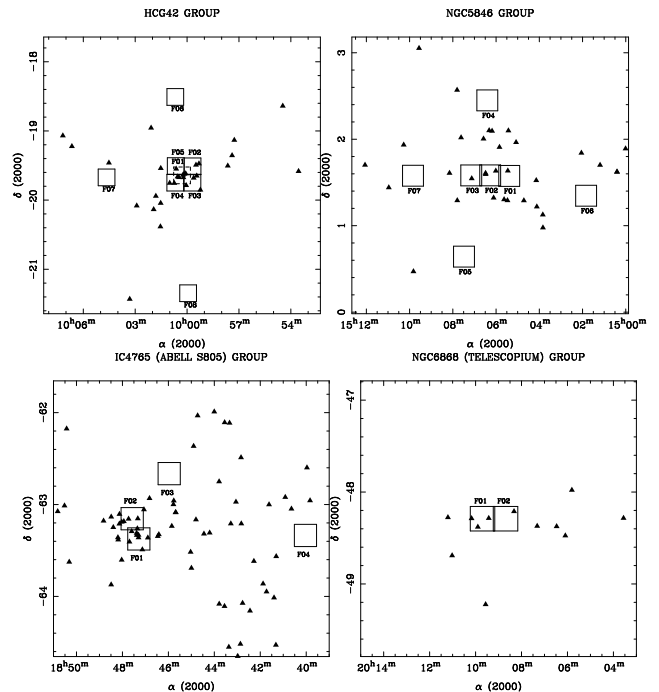


FIG. 1.— Projected distribution of all observed fields (squares) in the area of the groups HCG 42 (upper left), NGC 5846 (upper, right), IC 4765 (lower, left) and NGC 6868 (lower, right). The triangles indicate all previously catalogued member galaxies with known redshifts in the area of each group. The size of each plot is  $\sim 3 \times 3 \text{ deg}^2$ , except for HCG 42 where the size is  $\sim 4 \times 4 \text{ deg}^2$ .

member galaxies of the groups with previously known redshifts (solid triangles). We have used the SExtractor software (Bertin & Arnouts 1996) to detect the objects and to obtain the photometric parameters. All co-added images were previously processed by removing all bright galaxies and saturated stars. Saturated stars were masked and replaced by the median value of the nearby sky, while the bright galaxies were extracted from the frames by fitting their isophotes using the STSDAS.ISOPHOTES.ELLIPSE and BMODEL programs. When there were remaining residuals from the galaxy subtraction process, specially in cases where elliptical isophotes were a poor fit to the profile of the galaxy, we simply masked the region and replaced the pixels by the median nearby sky value.

We have processed the CCD images at the telescope, with the IRAF<sup>1</sup> package, using the data pipeline scripts written specifically to reduce the data product obtained with the Warsaw telescope. The data have been bias/overscan-subtracted and trimmed. Twilight flats in V and I were observed at the beginning and at the end of each night. Flatfield images were combined in order to make a master flat which was then used to flat field the data. The images were registered to a common position and combined by obtaining their median value at each pixel. The final combined images show, on average, an *rms* pixel-to-pixel variation of 1.2% and 0.8% in the V- and I-band respectively.

Calibrations of the magnitudes to the standard system were derived using observations of standard stars from Landolt (1992). The tasks APPHOT and PHOTCAL

<sup>1</sup> IRAF is distributed by NOAO, which is operated by the Association of Universities for Research in Astronomy Inc., under contract with the National Science Foundation.

were used to determine the instrumental magnitudes, to determine the aperture corrections and to derive the transformation between the instrumental and standard systems. The calculated coefficients associated to the color terms were small and very stable during the nights. The zero points were calculated assuming a color index of  $(V - I) = 1$ , a typical value for low surface brightness dwarf galaxies in nearby groups and clusters like Virgo (see for example Impey & Bothun 1997; Carrasco et al. 2001).

### 3.1.1. Detection and photometry

We have used the V-band images for object detection and to extract the main photometric parameters. The photometry in the I-band images were performed using the parameter ASSOC, i.e. the main photometric parameters were extracted only for those objects detected in the V-band images. The resulting catalogs were then matched to generate a master catalog per group. All objects with a fixed surface brightness threshold of 25.8 mag/arcsec<sup>2</sup> ( $\sim 1.1\sigma$  above the sky level) and with a minimum area of 10 pix<sup>2</sup> in V-band images were found and their main photometric parameters obtained. Note that the  $1.1\sigma$  above the sky level corresponds to a limiting surface brightness of  $\sim 25.8$ – $26.0$  V mag/arcsec<sup>2</sup> in the fields. We used a threshold of 25.8 mag/arcsec<sup>2</sup> in order to have a common surface brightness cut for object detection in all observed fields.

We decided to adopt the magnitude given by the parameters MAG\_AUTO as the total magnitude of the objects. This magnitude gives a more precise estimation of “total magnitude” for galaxies. The MAG\_AUTO is based on the Kron’s “first moment” algorithm (Kron 1980). For each object, elliptical apertures are chosen and the position angle and the ellipticity are defined by the second-order moments of the light distribution. The maximum aperture is then defined as one that has double the area of the isophotal elliptical aperture. Inside this aperture, the integrated light is used to construct a growth curve where the first moment is computed. The sensitivity level in magnitude is very similar in all groups. The completeness of our sample for point sources fall below 90% at magnitudes of  $V \sim 23$  mag and  $I \sim 22.5$  mag.

The colors were derived by measuring the fluxes inside a fixed circular aperture. The aperture was chosen to be slightly larger than the average seeing measured in the images. We used a value for the aperture of 3 arcsec in diameter in both filters.

The star/galaxy separation has been done using the “stellarity” flag. All objects with “stellarity” index  $\leq 0.35$  have been selected and flagged as galaxies. This chosen value is based on our previous work done in the Dorado Group (Carrasco et al. 2001) and supported by Monte Carlo simulations (see section 4.3). Galaxies which mimic Local Group low surface-brightness dwarf galaxies at the distance of the groups are classified in all cases with “stellarity” flags lower than 0.35. To check the classification we used two different approaches presented in Carrasco et al. (2001); using eye control and by plotting pairs of parameters (see section 2.4 in Carrasco et al. 2001). In both cases we found that  $\gtrsim 95\%$  of the object were classified identically as galaxies down to  $V = 21.5$  mag and  $I = 21$  mag. These results are in

agreement with those obtained from Monte Carlo simulations presented in section 4.3.

The final catalogs contain all galaxies brighter than  $V = 21.5$  mag. We used this magnitude cutoff due to the large uncertainties in the classification at fainter magnitudes. This imposed cutoff corresponds to absolute magnitudes  $M_V = -12.2$ ,  $-10.9$ ,  $-12.9$  and  $-11.6$  at the distances of HCG 42, NGC 5846, IC 4765 and NGC 6868 respectively.

### 3.1.2. Photometric errors

An accurate determination of the Galaxy Luminosity Function requires knowledge of any external or systematic errors that could be affecting the data. Because the groups were observed following a mosaic pattern, with a small overlap between consecutive images, we have used the objects detected in more than one field, to check the photometry and estimate the errors. We have compared the total magnitudes and the magnitudes within a fixed aperture, for all objects in the common regions. These comparisons are shown in Fig. 2. This figure shows the residual magnitudes as a function of the magnitude (total/fixed aperture). The residuals for the galaxies in the four groups are, on average,  $\sim 0.05$  mag for  $V \leq 20$  mag, with an *rms* of the residual of the same order. For fainter magnitudes and  $V \leq 21.5$  mag, the scatter is higher and the average difference is  $|\Delta(V)| < 0.1$  mag. For magnitudes fainter than  $V = 21.5$  the difference is greater than 0.3 mag. These results are in agreement with the simulations presented in section 4.3.

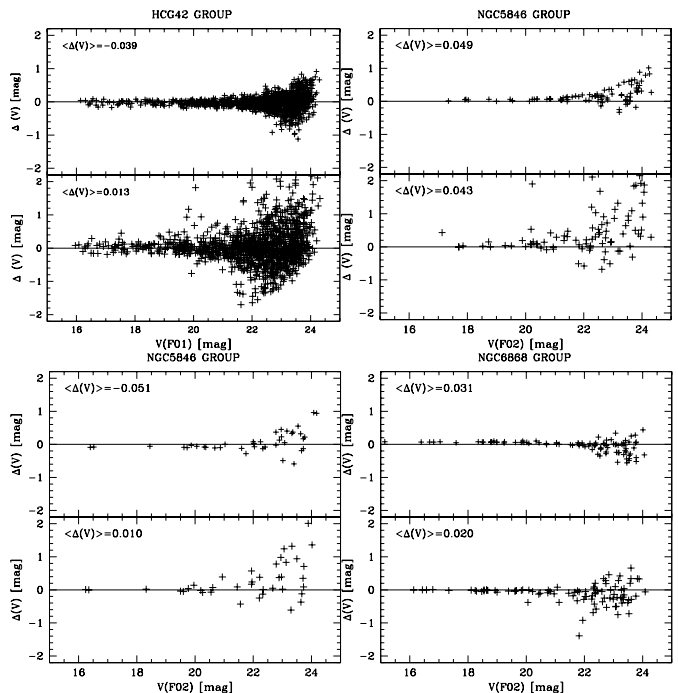


FIG. 2.— Differences in magnitude as a function of the total/aperture magnitudes for all objects observed in common in the overlapping regions of HCG 42 (top, left), NGC 5846 (top, right), IC 4765 (bottom, left) and NGC 6868 (bottom, right). On average, the difference is  $\sim 0.05$  for objects with  $V \leq 20$  mag.

The galaxy catalogs have then been used to select the dwarf galaxies with surface brightnesses, luminosities and scale lengths similar to the dwarf spheroidal galaxies

present in the Local Group and to select the galaxies for spectroscopic follow up.

### 3.2. Spectroscopy

In addition to the imaging of the groups we have performed a spectroscopic follow up of galaxies in the group cores. The spectra of the galaxies in these central regions were observed with the Wide Field CCD Camera (WFCCD), mounted on the 2.5 m Du Pont telescope in the Las Campanas Observatory in Chile. The spectra were obtained in two different sessions, during the nights of June 18 – 22, 1999 and March 9–12, 2000, in dark conditions, with a good transparency and under relatively good seeing (typically between 1.2 and 1.5 arcsec). The WFCCD camera is a CCD imager and a spectrograph capable to take images and multi-slit spectra in a 25-arcmin diameter field of view with a pixel size of 0.774 arcsec. The galaxies have been observed using a low-resolution grism, giving a wavelength coverage of roughly 3800Å–7400Å with a dispersion of  $\sim 4\text{\AA}/\text{pix}$  and a resolution of  $\sim 8\text{\AA}$ .

All galaxies with apparent magnitudes brighter than  $V=20$  were selected for spectroscopy and several masks were designed for the observations of the galaxies in each group. The spectroscopic sample included all galaxies detected and classified as low-surface brightness dwarf galaxies (see section 4.1) and many of the brightest galaxies of each of the groups. A total of 669 galaxies were selected for spectroscopic observations (225 galaxies in the area of HCG 42, 184 galaxies in the area of NGC 5846, 169 galaxies in the area of IC 4765 and 91 galaxies in the area of NGC 6868) distributed in 29 masks. To keep the wavelength coverage between  $\sim 3800\text{\AA}$  and  $7400\text{\AA}$ , the objects in the masks were placed within  $\pm 6$  arcmin from the nominal masks centers. To maximize the number of objects per mask, a minimum separation of 1 arcsec was used between slits. The objects were placed with a minimum distance of 10 arcsec from the slit edges in order to have enough pixels covered by sky, for a good sky subtraction. The slit width was set to 1.5 arcsec (June 1999 run) and 1.94 arcsec (March 2000). Unfortunately, two of the five nights in the 1999 run and one of the four nights in the March 2000 run were lost due to bad weather conditions. This affected the observational coverage in the area of the IC4765 and NGC 6868 groups.

Bias, dome and sky flats (for illumination correction) were observed for each night of observation. Helium-neon comparison lamps were observed before and after each exposure, to allow wavelength calibration of the spectra. Masks containing bright galaxies were typically observed for 40 minutes to 1 hour. For masks with fainter objects, the total exposure times were typically 1.5 to 2 hours.

A set of scripts, running under IRAF, were written to reduce the spectra. All two dimensional images were bias/overscan subtracted. The science frames and their corresponding flats and comparison lamps were cut into separate images. Each slit spectra were then flat-fielded using a normalized flat. The normalization of the flats was done by fitting a cubic spline of order 25. After flatfielding, a region was selected to extract the sky. The sky subtraction was done adjusting a low order chebyshev polynomial (typically of order 1 or 2). The spectra were ex-

tracted using an aperture of two times the full-width half maximum of the spectral profiles. The comparison lamps were extracted using the same fitting parameters we used to extract the object spectra. The wavelength calibration was performed using between 20 and 30 lines identified in the He-Ar comparison spectra. All calibrated spectra have an *rms* of the fit less than  $0.1\text{\AA}$ . Finally, the residual of the sky-subtraction (typically, the sky lines at  $5577.35\text{\AA}$ ,  $6300.23\text{\AA}$  and  $6362.80\text{\AA}$ ) were cleaned from the spectra by hand. We obtained a final spectral resolution of  $\sim 8\text{--}10\text{\AA}$  at  $6000\text{\AA}$  (measured from the FWHM of the arc and sky lines). Spectra observed more than once were then combined by the median. An example of the spectra is shown in Fig. 3. The figure shows the co-added spectra of two newly discovered dwarf elliptical galaxies detected in the central region of the poor cluster IC 4765.

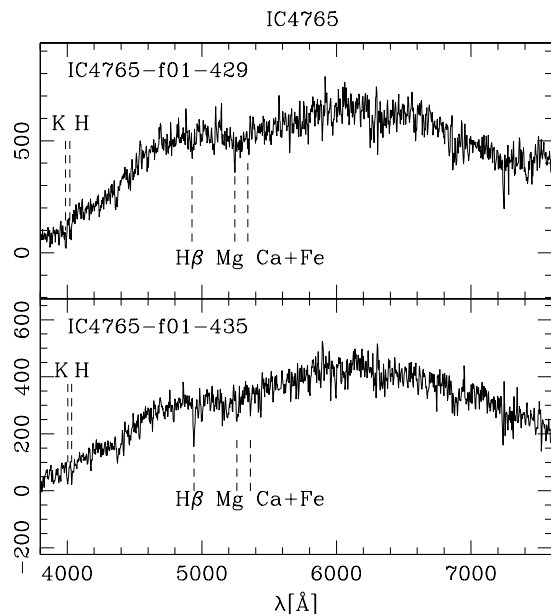


FIG. 3.— Spectra of two newly discovered dwarf elliptical galaxies in the central region of IC 4765, IC4765-f01-429 (upper panel) and IC4765-f01-435 (lower panel). The galaxies have apparent magnitude of  $V = 16.8$  and  $V = 17.1$  ( $M_V = -17.43$  and  $M_V = -17.13$ ) respectively. The main absorptions lines detected in the spectra are marked. The y-axis is in arbitrary units.

#### 3.2.1. Completeness of the Spectroscopic sample (selection function)

With the photometric and spectroscopic catalogs constructed from the observations it is possible to determine the completeness in magnitude of the spectroscopic sample. This completeness or selection function is an important factor that has to be taken into account in the determination of the Group Galaxy Luminosity Function. Fig. 4 shows the histogram of the total magnitude distribution in  $V$  (corrected by interstellar extinction) for all galaxies brighter than 21 mag presented in the photometric catalogs and for all galaxies with known radial velocity presented in the observed area (shaded histogram). For HCG 42 and IC 4765, the completeness fractions are 100% for  $V \leq 17.5$  mag and drop to  $\sim 70\%$  between  $17.5 < V \leq 19.8$  mags. In NGC 5846, the completeness fraction is 100% for  $V \leq 16$  mag and  $\sim 65\%$

for  $V \leq 19$  mag. Finally, for NGC 6868 the completeness is 100% for  $V \leq 17$  mag and  $\sim 70\%$  for  $V \leq 18.5$  mag. For magnitudes fainter than  $V = 18$ , the completeness fraction is an upper limit because the bins were not corrected by incompleteness in the detection of the LSB galaxies determined in section 4.3.

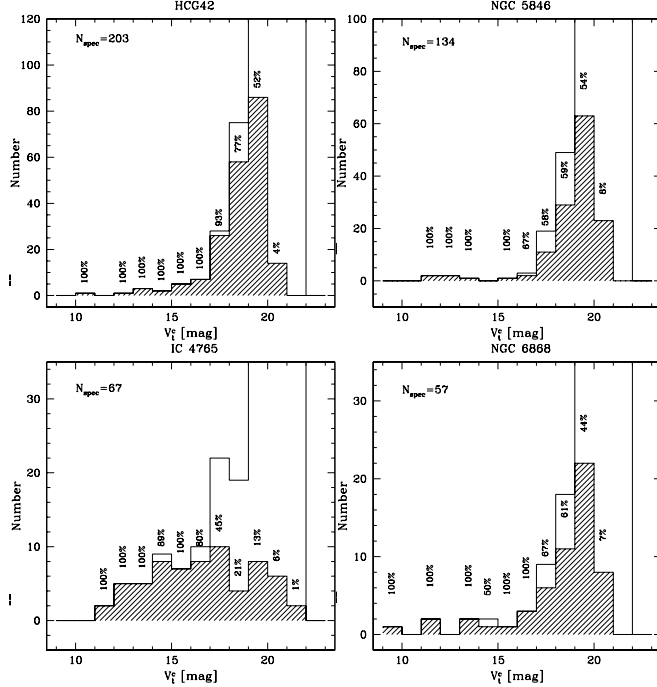


FIG. 4.— Histogram of the total magnitude distribution for all galaxies presented in the photometric catalogs with  $V \leq 21$  mag (open histogram) and for all galaxies with radial velocities (shaded histogram). For each group the completeness fraction is given in percentage. The number  $N_{spec}$  in each group includes the galaxies with radial velocities from other source and inside of our observed fields.

#### 4. PHOTOMETRIC ANALYSIS

##### 4.1. Selection of the Low surface-brightness dwarf galaxies

Low surface-brightness dwarf galaxies in the area of the four groups were searched for by applying a similar criteria to that used in Carrasco et al. (2001), for the Dorado group. As a first approach, we are interested in searching for galaxies that have similar magnitudes, sizes and surface brightnesses to those of the dwarf galaxies observed in our own Local Group. Fig. 5 shows the distribution of the Local Group dwarf galaxies in the  $M_V - \mu_V$  plane as they would be seen at the distance of NGC 5846 and IC 4765 groups (the closest and most distant groups in our sample). The magnitudes, scale lengths and central surface brightnesses of Local Group galaxies were taken from Mateo (1998) and references therein. As we can see in the figure, at the distance of NGC 5846 ( $24.1 h^{-1}$  Mpc), we do not expect to detect galaxies like Draco, Carina and Sextans A, because these galaxies are too faint and below the survey detection limit of  $\mu_{lim} = 25.8$  V mag/arcsec<sup>2</sup> (the dashed line indicate the limiting absolute magnitude corresponding to an apparent magnitude of  $V = 21.5$  mag at the distance of the groups). However, galaxies like Antlia would be possible to identify, following the same smoothing method applied for the

galaxies in the Dorado group (Carrasco et al. 2001). In IC 4765, only the brightest dwarf galaxies, like Fornax, may be possible to be detected at the distance of this group.

The selection criteria applied to detect the LSB galaxies involve the parameters given by the exponential profile fit: the central surface brightness, the scale length and the limiting diameter.

The galaxy radial profile can be represented by a generalized exponential profile or Sersic law (Sérsic 1974) of the form:

$$\mu(r) = \mu_0 + 1.086(r/h)^n, \quad n > 0 \quad (1)$$

where  $\mu_0$  is the extrapolated central surface brightness,  $h$  is the scale factor and  $n$  is the generalized exponent. For disk galaxies and dwarf fainter than  $M_V \sim -17$ , the surface brightness profile is well fit by a pure exponential law, with  $n = 1$ .

For each of the eight isophotal areas given by SExtractor, we determined the surface brightness and the radius at a given isophotal area as  $\mu_i = \mu_{peak} \times i/8 + (1 - i/8) \times \mu_{lim}$  and  $r_i = \sqrt{A_i \epsilon / \pi}$ , where  $\mu_{peak}$  is the surface brightness at the pixel of maximum intensity,  $\mu_{lim}$  is the surface brightness at the limiting isophote,  $\epsilon = a/b$  is the elongation and  $A_i$  is the isophotal area at the  $i$ -label.

We used  $\mu_0$  and  $h$  given by the fit as the main parameters to allow a primary cut for the LSB's selection. All galaxies with  $\mu_0$  fainter than  $22.5$  V mag/arcsec<sup>2</sup> and  $h > 1.5$  arcsec were selected (note that the values for the scale factors used here are slightly larger than the mean seeing value obtained for the images). The cut in scale length corresponds to a physical size of  $\sim 0.4 h^{-1}$  kpc,  $\sim 0.18 h^{-1}$  kpc,  $\sim 0.4 h^{-1}$  kpc and  $\sim 0.24 h^{-1}$  kpc at the distance of HCG 42, NGC 5846, IC 4765 and NGC 6868 groups respectively and is comparable to the scale length cut used for the LSBs selection in the Dorado group.

A second cut was done using the limiting diameter which can be represented by the parameters given by the exponential fit, in the following form

$$\theta_{lim} = 0.735(\mu_{lim} - \mu_0)10^{0.2(\mu_0 - m_{tot})} \quad (2)$$

where  $\mu_{lim}$  is the surface brightness at the limiting isophote of  $25.8$  V mag/arcsec<sup>2</sup>,  $\mu_0$  is the extrapolated central surface brightness,  $m_{tot}$  is the total magnitude of the objects, and  $\theta_{lim}$  is in arcsec. All galaxies with a physical diameter at the limiting isophote larger than  $1.2 h^{-1}$  kpc were selected as LSB candidates. This is the same physical diameter we used to select the LSB galaxies in the Dorado group and corresponds to an apparent size of  $4.5''$ ,  $10''$ ,  $4''$  and  $7.5''$  at the distance HCG 42, NGC 5846, IC 4765 and NGC 6868 respectively. After the selection, all galaxies were visually inspected. A few galaxies were discarded based on the *flag* of the photometric quality given by SExtractor (see Bertin & Arnouts 1996, for details). Objects with *flag*  $> 0$  have a bright object in their proximity (the additional contaminating light from the nearby bright source can “create” false LSB's) and were not included in the final LSB catalog.

A total of 71 LSB galaxy candidates were detected using the cut applied above (32 in HCG 42, 14 in NGC 5846, 15 in IC 4765 and 10 in NGC 6868). Three LSB



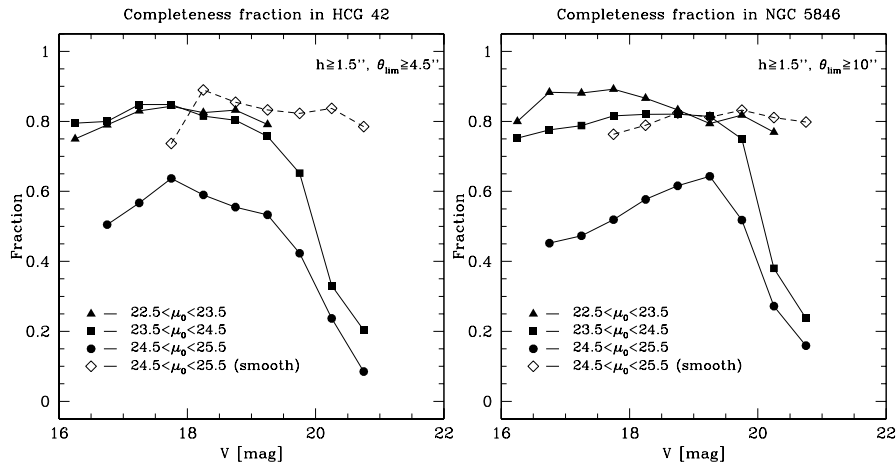


FIG. 6.— Completeness fraction as a function of the total magnitude in V for simulated galaxies at the distance of the groups HCG 42 (left) and NGC 5846 (right). The different symbols correspond to different central surface brightness bins. The open symbols represent the completeness fraction in the last bin where we used the smoothed technique to search LSB galaxies.

the last column of Table 3.

The photometric data and the profile-fitting parameters of the LSBs detected in the groups are shown in Table 3. The table is arranged as follow: (1) galaxy identification, given by the name of the group, followed by the field name and the galaxy number. Those galaxy numbers starting with "L" are the very low surface-brightness galaxies detected using the smoothing technique; (2) and (3) equatorial coordinates; (3) total V-magnitude; (4) absolute V-magnitude calculated assuming the distances given in Table 1; (5)  $(V - I)$  colour inside an aperture of 3 arcsec; (7) Isophotal diameter at 25.8 V mag/arcsec<sup>2</sup>; (8) limiting diameter; (9) extrapolated central surface brightness; (10) the scale factor; (11) and (12) the effective radius and mean effective surface brightness; (13) morphological classification.

#### 4.3. Photometric detection efficiency and errors

In order to determine the efficiency of our method to detect the LSB galaxies, to estimate the photometric errors and the errors in the calculation of the profile-fit parameters (extrapolated central surface brightness, scale factor and limiting diameter) a series of add-star experiments and Monte Carlo simulations were done.

The simulations were performed on the science frames in order to have the same characteristics of a real image (cosmetic defects, crowded images, light gradients, noise and seeing). The LSB galaxy detection efficiency was determined as  $f(V_t, \mu_0) = n_{det}/n_{gen}$ , where  $n_{det}$  is the number of galaxies detected by SExtractor and  $n_{gen}$  is the number of galaxies generated. We computed the efficiency for galaxies with magnitudes, central surface brightnesses and scale lengths typical of low surface-brightness dwarf galaxies at the redshift of the groups. We generated galaxies with exponential profiles with different scale lengths, central surface brightnesses, random ellipticities and position angles and placed them onto the frames. Each image was convolved with a point spread function constructed from bright, non-saturated stars in the frame. We generated 400 galaxies with exponential profiles in bins of 1 mag/arcsec<sup>2</sup> and between  $22.5 < \mu_0 < 25.5$  mag/arcsec<sup>2</sup> in central surface brightness. The galaxies were generated in groups of 20 (five for the brightest magnitude bins), randomly distributed over the field, and with magnitudes between

16.0 – 21.0 mag (in bins of 0.5 magnitudes). These galaxies were created using the MKOBJECTS program in the NOAO.ARTDATA package in IRAF.

We ran the SExtractor program using the same detection parameters previously used for the real-galaxy detection (see section 3.1.1). The common objects in the input and output catalogs were matched. Using the eight isophotal areas, for each matched galaxy we calculated the central surface brightness, scale length and the limiting diameters as in section 4.1. The resulting values were then compared with the input values. For the last bin in surface brightness, we repeated the simulations, but using the smoothed technique described in section 4.2.

The completeness fraction in the detection of the LSB galaxies in the interval of  $22.5 < \mu_0(V) < 25.5$  is shown Fig. 6. The completeness is  $\sim 80\%$  for  $V \leq 20$  and  $\mu_0 \leq 24.5$  V mag/arcsec<sup>2</sup>. For fainter magnitudes the detection fraction drops rapidly. For the last interval in surface brightness, the detection fraction is below 50%. However, using the optimized method (smoothing technique) described in section 4.2, the fraction goes up to  $\sim 80\%$ .

Fig. 7 shows the difference between the input and output magnitudes (left plot) and the difference in scale factor (upper right panel) and central surface brightness (lower right panel) as a function of total magnitudes for the recovered simulated galaxies. The difference in magnitude for galaxies with  $\mu_0 \leq 24.5$  mag/arcsec<sup>2</sup> is of the order of 0.2 mag, and increases to 0.5 mag in the last central surface brightness bin. In the case of the central surface brightness, the difference is, on average, 0.5 mag/arcsec<sup>2</sup>. There is a tendency that for magnitudes brighter than 19 mag in V, the central surface brightness values are underestimated, while for fainter magnitudes the tendency goes in the opposite sense, i.e. the calculated central surface brightness values are overestimated. However, the difference in surface brightness is negligible compared to the errors. In the case of the scale factors, we note a clear tendency for the calculated values to be overestimated. For  $V < 19$  mag and  $\mu_0 < 24.5$ , the scale factors are overestimated in about 30%. For the last surface brightness bin, these differences are  $\sim 60\%$ . There is a clear limitation in estimating in a correct way the scale length of the real galaxies, especially at small sizes. This means that the values of scale lengths listed in Table 3



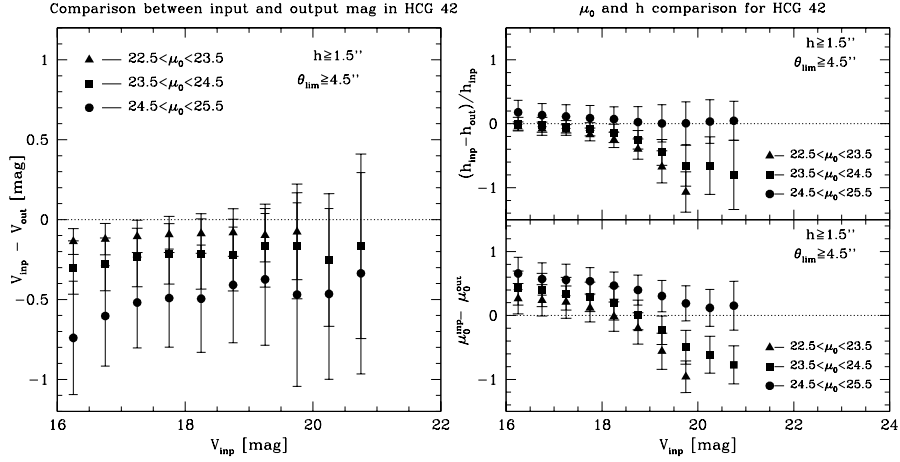


FIG. 7.— Difference in magnitudes (left panel) and in central surface brightness and scale factor (right panel, bottom and top) for recovered simulated galaxies. The galaxies presented here were simulated in one of the observed control field in the area of HCG 42 group.

for  $h < 2''$  and fainter than  $V \sim 20$  mag are only upper limits.

We also estimated the completeness of the sample by adding point sources from the observed point spread function of the frames using ADDSTAR in the DAOPHOT package, inside IRAF. A total of 1000 stars per 0.5 mag bin and between  $15 < V < 24$  mag were generated. The recovery fraction was then compared with the input and the completeness and the differences in magnitudes were computed. The completeness limit for point sources with “stellarity index”  $\geq 0.9$  is  $\gtrsim 90\%$  down to our limit of  $\sim 23$  mag in  $V$ . This result is in agreement with the limiting magnitude derived in section 3.1.1. The difference between the input and output values magnitudes is  $|\Delta(V)| \sim 0.06$  mag. This is not surprising, since the Kron’s “first moment” algorithm, used to calculate the total magnitude, measures about 95% of the flux for objects with stellar profiles and about 90% for galaxies with exponential profiles (Infante & Pritchet 1992).

## 5. SPECTROSCOPIC ANALYSIS

### 5.1. Radial velocities

The radial velocities were determined using two different methods. For spectra with emission lines, the routine RVIDLINE in the IRAF RV package was used employing a line-by-line gaussian fit. For spectra dominated by absorption lines, the XCSAO cross-correlation algorithm in the IRAF RVSAO package (Kurtz et al. 1992) was used. The observed absorption spectra were correlated with twelve high signal-to-noise stellar and galaxy templates. The  $R$  values (see Tonry & Davis 1979) were used to evaluate the reliability of the measured velocities. For  $R > 4$ , the template which gave the lowest error was used to derive the radial velocity. This method gave more consistent results than other combinations we tried, such as a mean of the results of the twelve correlations. For  $R \leq 4$ , we inspected the spectra and tried line-by-line gaussian fitting to check which were the most reliable cross-correlation results.

We were able to measure the radial velocities for 412 of 669 galaxies selected for spectroscopic observations ( $\sim 62\%$  of the sample). This corresponds to  $\sim 83\%$ ,  $\sim 68\%$ ,  $\sim 53\%$  and  $\sim 62\%$  of the selected objects in the area of HCG 42, NGC 5846, IC 4765 and NGC 6868 re-

spectively. The final radial velocities are shown in Table 4. The table lists the following parameters: (1) galaxy identification as in Table 3; (2)–(3) RA and DEC for the group; (4)  $V$  total magnitudes; (5)  $(V-I)$  colour inside an aperture of 3 arcsec; (6) galaxy radial velocities corrected to the heliocentric reference frame; (7) radial velocity errors; (8)  $R$  values (real numbers) or the number of emission lines (integer value) used to calculate the velocities; (9) flag for galaxies with multiple measurements: “0” – value has been discarded, “1” – value has been included in the calculation of the final radial velocity; (10) final radial velocity. For galaxies with multiple measurements, these values are the mean weighted velocity (see below); (11) final radial velocity error yielded by the RVSAO/RVIDLINE packages and by the error of the weighted mean velocity in the case of multiple measurements.

In column 6, besides the heliocentric radial velocity, we also included the radial velocities available in the literature. The identification and references are shown in the last column of the table. For galaxies with multiple radial velocity measurements, we derived the mean weighted velocity following Quintana, Carrasco & Reisenegger (2000). These velocities are calculated using the following relation:

$$\bar{V} = \frac{\sum_i w_i v_i}{\sum_i w_i} \quad (3)$$

where  $v_i$  is the galaxy velocity,  $w_i = 1/\sigma_i^2$  is the weighting factor, and  $\sigma_i$  is the uncertainty. The weighting factor  $w_i$  came from our internal uncertainties (col 7 in Table 4) or from the published uncertainties. The error of the weighted mean velocity for galaxies with multiple measurements is given in column 11 in Table 1 (see Quintana, Carrasco & Reisenegger 2000, for a full discussion of the criteria used to calculate the errors of the weighted mean velocities).

### 5.2. Estimating the internal and external errors

Those absorption spectra for which radial velocities could be measured both by using a line-by-line gaussian fit and cross-correlation were used to estimate the internal errors. In Figure 8 (top panel) we show the radial velocity differences of 187 galaxies (cross-correlation minus line-by-line) as a function of the square root of the sum

of the quadratic errors. The average difference between both data sets is only  $10 \text{ km s}^{-1}$ , with an *rms* deviation of the residuals of  $\sim 100 \text{ km s}^{-1}$ . The average difference is negligible compared to the *rms* suggesting that the radial velocity errors given by the cross-correlation and/or by the line-by-line gaussian fit are underestimated and are larger than the values listed in Table 4. Therefore, we adopted the *rms* deviation of the residual of  $100 \text{ km s}^{-1}$  as the true radial velocity errors of our typical measurement for further analysis (determination of the velocity dispersion of the group).

We used the radial velocities obtained in common with the literature to estimate the velocity zero-point corrections (if needed) and any external error that could be presented in the dataset. We compared our radial velocities with the values published by Zabludoff & Mulchaey (1998, 2000) and de Carvalho et al. (1997) for HCG 42 and NGC 5846 groups, with Malamuth et al. (1992), Bell & Whitmore (1989) and Stein (1996) for IC 4765 group, and with Garcia (1993) and Ramella et al. (1996) for the NGC 6868 system. Also, for galaxies that were not presented in the references listed above, we compared our velocities with velocities from the NASA/IPAC Extragalactic Database (NED). The lower plot in Figure 8 shows the velocity differences for 23 galaxies observed in common with Zabludoff & Mulchaey (1998, 2000) (20 galaxies in HCG 42 and 3 in NGC 5846) as a function of the square root of the sum of the quadratic errors. We found a mean difference of  $-14 \text{ km s}^{-1}$  (dot-short dashed line) with an *rms* deviation of the residual of  $\sim 100 \text{ km s}^{-1}$ . The mean difference is consistent with the mean internal difference shown in the top panel of Figure 8. Similar results were obtained when we compared the data for the other two groups. Following these results, we did not apply any zero-point correction to the data.

For a few galaxies we found large discrepancies with respect to the values given in the literature. An example is the case of the background late-type galaxy H42-f04-1528. For this galaxy we obtained a radial velocity of  $44597 \pm 53 \text{ km s}^{-1}$ , while de Carvalho et al. (1997) and Zabludoff & Mulchaey (2000) obtained values of  $3931 \pm 33 \text{ km s}^{-1}$  and  $19233 \pm 80 \text{ km s}^{-1}$  respectively. The spectrum of this galaxy shows a strong  $H_\alpha$  emission line and clear absorption features that put the galaxy at the redshift calculated by us. In this case, we adopted our value as the radial velocity for this galaxy. For other similar cases, when the analysis of the spectra, the galaxy morphology, or other properties showed large discrepancies, we discarded the velocity and we did not use it into the calculation of the final radial velocity. Column 9 in Table 4 identifies which galaxies were used or not in the calculation of the final radial velocity.

In addition to the galaxies listed in Table 4, we have cross-correlated the positions of the galaxies in our photometric catalogs with available data in the literature to search for galaxies with radial velocities that were not included in our spectroscopic survey and are members of the groups. The result of this search included 17 galaxies in HCG 42, 8 in NGC 5846, 23 in IC 4765 and 1 in NGC 6868 groups. In cases where the galaxies had more than one radial velocity measurement available in the literature, we calculated the mean weighted velocity following equation 3.

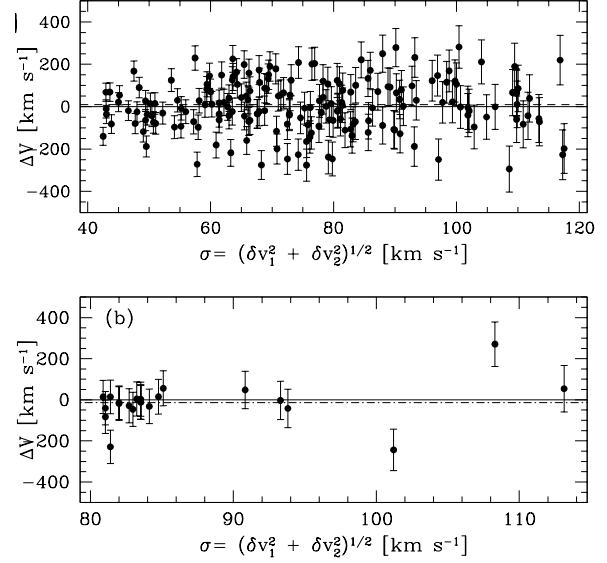


FIG. 8.— (a) Radial velocity differences of 187 galaxies measured using cross-correlation and line-by-line gaussian fits against the root square of the sum of the quadratic errors. The average difference in velocity (dashed line) is  $10 \text{ km s}^{-1}$  with an *rms* of the residual of  $100 \text{ km s}^{-1}$ . (b) Radial velocity differences for 23 galaxies in common with Zabludoff & Mulchaey (1998, 2000). In this case, the average difference in velocity is  $-14 \text{ km s}^{-1}$  with an *rms* deviation of the residual of  $100 \text{ km s}^{-1}$ .

### 5.3. Background objects among the LSB galaxies

We determined the radial velocity for eleven of the 80 LSB galaxies of our list, although we placed slits over 60 of them (note that due to the bad weather we were not able to obtain spectra for galaxies in four masks. These masks belong to the groups IC 4765 and NGC 6868 and contained the non-observed 20 LSB candidates). Six LSBs were found to have discordant redshifts and were therefore identified as background galaxies while 5 were identified as galaxy members of the groups: 3 in NGC 5846 and 2 in IC 4765. The background galaxies correspond to the field of HCG 42 (2), NGC 5846 (2) and NGC 6868 (2). Table 1 lists the main structural parameters and the radial velocities for the six background galaxies (first six rows) and for the five LSB galaxies (last five rows).

The two background galaxies in the direction of NGC 6868 are dwarf members of a second structure located at  $cz \sim 4900$  (i.e.  $2000 \text{ km s}^{-1}$  away of the group - see section 6.4). These two galaxies have low surface-brightnesses, absolute magnitudes and  $(V - I)$  colors typical for the LSB population. For the remaining four background galaxies, 2 have colors  $1.3 < (V - I) < 1.5 \text{ mag}$  and two are blue galaxies ( $(V - I) \sim 1 \text{ mag}$ ). Further visual inspection showed that these galaxies have an irregular morphology with knots indicating some star formation activity.

Emission lines are present in four of six background galaxies (no emission lines are presented in the two dwarf galaxies in the background of NGC 6868). Emission lines are also present in the three LSB galaxies members of NGC 5846 group (see Table 5). About 75% of our LSB sample have morphological types dE/dSph and therefore the radial velocity could not be obtained due to the low S/N absorption spectra they presented. Only 25%

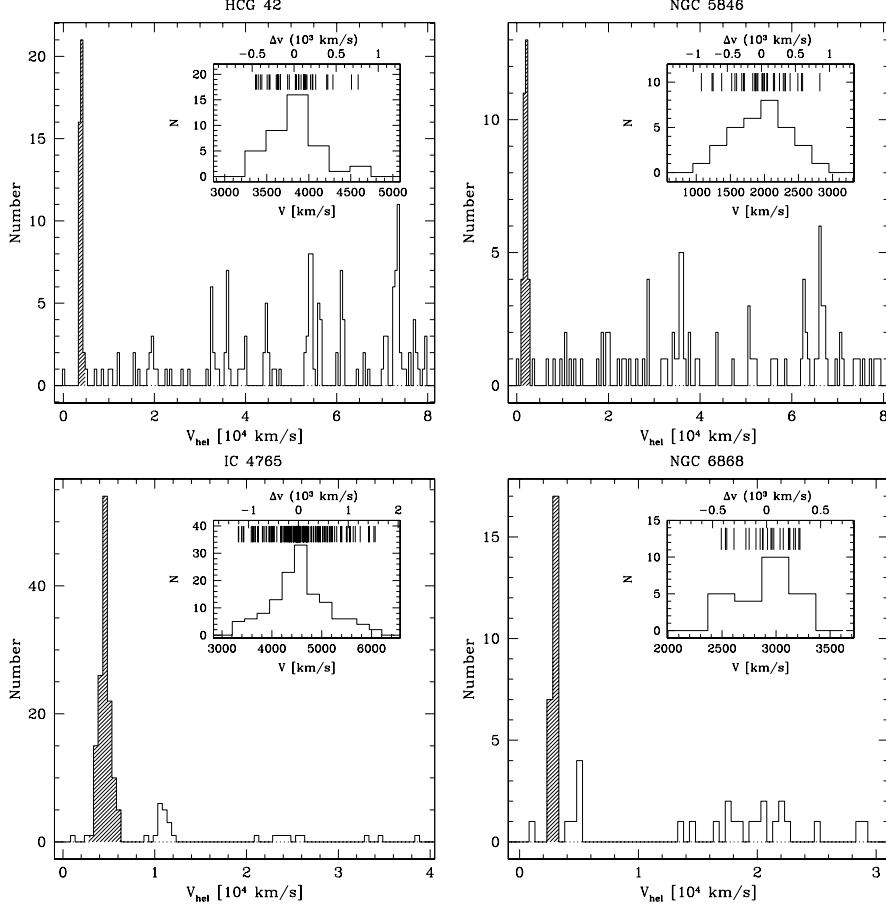


FIG. 9.— Velocity distribution histograms of all galaxies with measured radial velocities in HCG 42 (top left), NGC 5846 (top right), IC 4765 (bottom left) and NGC 6868 (bottom right) in bins of  $500 \text{ km s}^{-1}$ . The histograms also include those galaxies with radial velocities from the literature that were not observed in our survey. The shaded regions indicate all galaxies members of the groups. **Inset Figures:** velocity distribution of galaxies members of the groups. The bin size is  $250 \text{ km s}^{-1}$ . The tick marks at the top of the inset figures represent the velocities for individual galaxies.

of the sample are dwarf galaxies that show an irregular morphology and clear knots that indicate star formation activities (classified as dIrr). The four background emission line galaxies belong to this sub-sample. They represent only 30% of all galaxies we classified as dIrr. If we assume that the background galaxies are representative of this sub-sample, then we estimate that the fraction contamination of the sample is small ( $\lesssim 10\%$ ).

#### 5.4. Group velocity dispersion

We have used the 412 galaxies with radial velocities and the galaxies from the literature to derive the main dynamical parameters of the groups and to analyse the 3D galaxy distribution. Figure 9 shows the histograms of the velocity distributions for all galaxies with radial velocities in the area of the four groups. The shaded areas in the histograms show the location of the group galaxies (the velocity distributions of the galaxies members of the groups are shown in the inserted histogram in Fig. 9). We can clearly see several structures along the line-of-sight of the groups. In two groups, HCG 42 and IC 4675, we identified background structures associated to at least 2 and 1 clusters respectively. In the case of NGC 6868 there are evidences of a second structure located only  $2000 \text{ km s}^{-1}$  from the group. We discuss in more detail this point in section 6.4.

The average velocities and the one dimensional line-of-

sight velocity dispersions of the groups were calculated using the bi-weighted estimators of location and scale of Beer et al. (1990). We used an iterative procedure by calculating the location and scale using the ROSTAT program and applying a  $3\text{-}\sigma$  clipping algorithm to the results. We repeated this procedure until the velocity dispersion converged to a constant value.

The average group velocities and the corresponding velocity dispersions are tabulated in Table 1. We have also included in the table the results obtained for 3 new background structures detected in the area of the HCG 42 group and the poor cluster IC 4765. Table 1 contains the following information: (1) group ID; (2) and (3) equatorial coordinates of the group center (in all cases the brightest group galaxy); (4) total number of galaxies; (5) number of member galaxies; (6) average velocities; (7) velocity dispersion; (8) radius  $r_{200}$ .

Because the groups were observed at different physical areas, we decided to use the  $r_{200}$  radius as the estimator of the virial radius. In fact, analytical models (e.g. Gunn & Gott 1972) and numerical simulations (e.g. Cole & Lacey 1996) find that the radius  $r_{200}$ , defined as the radius in which the density is  $200\rho_c$  (critical density), contains almost all the virialized mass of groups and clusters. Then, the  $r_{200}$  is calculated assuming that  $M(r) \propto r$  and using the following relation:

$$r_{200} = \frac{\sqrt{3}\sigma_r}{10H_0(1+z)(1+\Omega_0z)^{1/2}} \quad (4)$$

where  $H_0 = 75 \text{ km s}^{-1} \text{ Mpc}^{-1}$ ,  $\Omega_0 = 0.2$ ,  $\sigma_r$  is the group velocity dispersion and  $z$  is the group redshift.

The average velocities and the velocity dispersions were calculated assuming an error for the galaxy velocities of  $100 \text{ km s}^{-1}$  determined in section 5.2. The results presented in the second line, for each group, were obtained using all galaxies with available radial velocities. On average, the velocity dispersions do not change, if we use only our data or the whole dataset (including the data from the literature).

## 6. PROPERTIES OF THE GALAXIES IN THE STUDIED GROUPS

### 6.1. The magnitude-surface brightness relation

It is well known that dwarf galaxies follow a tight magnitude-surface brightness relation (the central surface brightness increases with increasing luminosity) in clusters (e.g. Fornax; Hilker, Mieske & Infante 2003; Infante et al. 2003) and in groups (e.g. NGC 5044; Cellone & Buzzoni 2005). However, the validation of this relation has been questioned by a number of authors that argued against the existence of a magnitude-surface brightness relation for dwarf galaxies (Phillipps, Davies & Disney 1988; Irwing et al. 1990; Deady et al. 2002). It has been argued that the photometric sequence seen for dwarf galaxies in the  $M_V - \mu_0$  plane could be produced by selection effects. Very compact, high surface brightness galaxies as well as extended, very low surface-brightness galaxies in general are not present in the relation due to observational biases (Ferguson & Binggeli 1994; Impey & Bothun 1997).

In the last few years a large number of extended, very-low surface brightness objects were discovered in different environments (e.g. Virgo, Fornax, Leo I and Dorado: Impey et al. 1988; Bothun et al. 1991; Flint et al. 2001; Carrasco et al. 2001). On the other hand, very faint, high surface brightness objects were only recently discovered, in the Fornax (UCD - Ultra Compact Dwarf; Drinkwater & Gregg 1998; Drinkwater et al. 1999; Hilker et al. 1999) and Virgo (Jones et al. 2006) clusters. Both types of galaxies will fill the areas in the parameter space that were completely empty before, suggesting that there is no observed correlation between surface brightness and magnitude.

The sky brightness imposes a severe limitation in the correct determination of the luminosity distribution of galaxies. Therefore, extended, very low surface-brightness galaxies are very difficult to detect. The use of the smoothing technique described in section 4.2 gave us the possibility of finding several, previously undetected low surface-brightness galaxies. Fig. 10 shows the  $M_V - \mu_0$  relation for all LSB galaxies detected in the four groups (we excluded the 6 galaxies detected as background objects). We find no clear correlation between the central surface brightness and magnitude in Fig. 10, suggesting that the observed correlation noted by other several recent studies could be produced by a selection effect. Similar results are found in Dorado (Carrasco et al. 2001) and in Fornax for spectroscopically confirmed dwarf galaxies (Deady et al. 2002). Note that the ab-

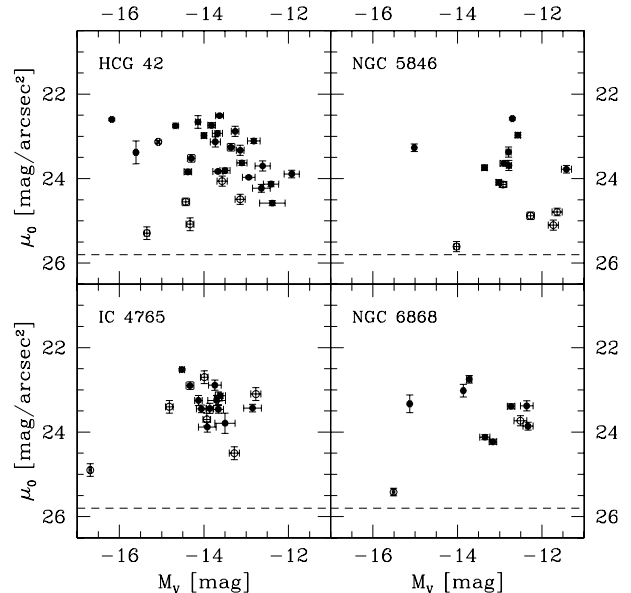


FIG. 10.— Absolute Magnitude - Central surface brightness relation for LSB galaxies in the area of HCG 42, IC 4765, NGC 5846 and NGC 6868 groups (filled circles). The extended, very-low surface brightness galaxies detected using the technique described in section 4.2 are represented by open circles. The limiting surface brightness of  $25.8 \text{ mag/arcsec}^2$  is represented by a dashed line.

sence of galaxies in the upper right region, where the M32-like objects and UCD galaxies are presented, is basically due to the limitation imposed by the seeing and the CLASS\_STAR used to select the dwarf galaxies.

### 6.2. LSB colors and color-magnitude relation

The sample of LSB galaxies has colors between  $0 < (V - I) < 1.5$  with a peak at  $V - I \sim 1 \text{ mag}$ . The peak is similar to the value derived for LSB galaxies in other nearby groups and in the field (see Carrasco et al. 2001, for details). About 56% of our sample is formed by blue galaxies ( $V - I < 1 \text{ mag}$ ) and only  $\sim 10\%$  of the sample is formed by very blue galaxies ( $V - I < 0.5$ ). This is expected since in low density environments of bright galaxies the blue LSB galaxies are more numerous than in dense environments (e.g. Coma Secker, Harris & Plummer 1997).

Fig. 11 shows the color-magnitude diagrams for all detected galaxies in the observed areas of the four groups. In the figure, the filled circles are the LSB galaxies detected in the groups. The extended, very low surface brightness galaxies were not included because no color information is available for them (they were detected in the V-band images only). Also in these plots we added all group galaxies with known redshifts (triangles).

The early-type galaxies present a well-defined sequence in the CMD diagram for more than 10 magnitudes in clusters (e.g. Fornax and Coma: Hilker, Mieske & Infante 2003; Adami et al. 2006). In Fig. 11 we note that this relation is also preserved in groups. The color-magnitude relation for early-type galaxies in groups extends to the region where the LSB galaxies (dSph, dE, dIrr) dominate. In all cases, except for some outliers, the LSB galaxies follow a well defined color-magnitude relation (only at fainter magnitudes, they become bluer). This result will have implications for the evolutionary scenarios of dwarf galaxies. A detailed analysis and discussion

of this point will be presented in a separate paper.

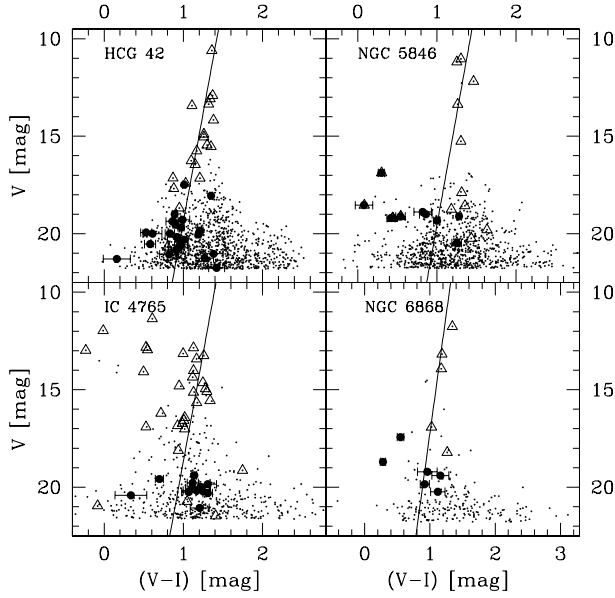


FIG. 11.— Color-magnitude diagrams of all galaxies brighter than  $V = 22$  (small dots) identified in the field of HCG 42 (upper left), NGC 5846 (upper right), IC 4765 (lower left) and NGC 6868 (lower right). The open triangles are the galaxies with known redshifts and the filled circles are LSB galaxies with color information. The solid line is the best fit to a subsample of our group data (triangles and filled circles) for which  $0 < (V - I) < 1.5$  mag.

### 6.3. Number density of the LSB galaxies

A detailed analysis of the spatial densities and radial distributions of dwarf galaxies provides important constraints on the various physical processes which are important in understanding galaxy formation. In addition, the analysis of the clustering properties of the dwarf galaxies is also important from the cosmological point of view. The distribution of satellite galaxies could indicate how luminous and dark material are distributed at different scales, and therefore can serve as a useful test for CDM (Cold Dark Matter) models of galaxy formation. Moreover, it may be used as good tracer of the dynamic evolution of the dark halos around bright galaxies.

The dwarf galaxy sample studied here extends from the center of the groups to a physical distance of  $< 0.5 h^{-1}$  Mpc, covering mainly the central regions. Fig. 12 shows the projected number density (in units of  $h^2 \text{ kpc}^{-2}$ ) as a function of the distance to the group centers for all LSB galaxies detected in the four groups. The data have been divided in bins of  $75 h^{-1} \text{ kpc}$ .

In the figure we clearly see a concentration of LSB galaxies towards the center of the four groups in a scale of  $< 250 h^{-1} \text{ kpc}$ . The projected number density at the largest measured bin of radius is similar to the value found in our control fields (represented by the dashed lines in the figure). Note that if our sample were dominated by background galaxies, then one would expect an almost flat distribution. The results shown in Fig. 12 clearly suggests that these galaxies are physically associated to the groups.

We fitted the number density profile of the LSB sample in Fig. 12 with a power law of the form  $\Sigma(r) = Ar^\beta$

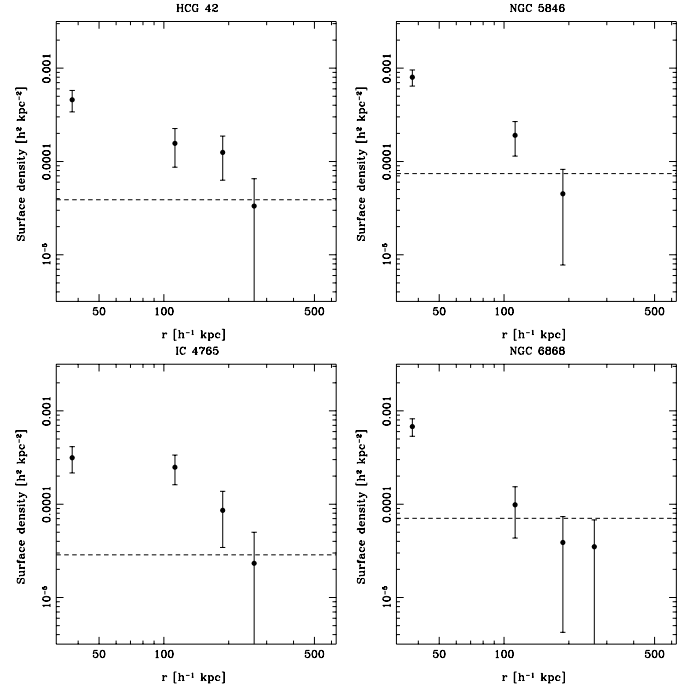


FIG. 12.— Projected number density of LSB galaxies as a function radius from for HCG 42 (top left), NGC 5846 (top, right), IC 4765 (bottom, left) and NGC 6868 (bottom, right). The group centers correspond to the position of the Brightest Group Galaxy of each group. The data has been divided in bins of  $75 h^{-1} \text{ kpc}$ . The dashed lines represent the number density in the control fields.

within a radius of  $250 h^{-1} \text{ kpc}$ . The last-square fit to the data gives a slope,  $\beta$ , of  $-1.27 \pm 0.21$ ,  $-1.75 \pm 0.15$ ,  $-1.48 \pm 0.29$  and  $-1.54 \pm 0.06$  with a correlation coefficient 0.932, 0.978, 0.900 and 0.995 for HCG 42, NGC 5846, IC 4765 and NGC 6868 groups respectively. These results are in agreement with those obtained by Vader & Sandage (1991) for satellite of isolated bright elliptical galaxies ( $\beta = -1.22 \pm 0.05$ ). Also, the results are in a good agreement with the results presented by Chen et al. (2005). These authors derived a best fit power-law of  $\beta \sim -1.6$ , after performing interloper contamination corrections, using a volume- and flux-limited Sloan Digital Sky Survey (SDSS) spectroscopic sample of galaxies.

We used the velocity catalog of member galaxies and the catalog of LSB galaxies to investigate the environmental dependence of the dwarf galaxies at scales of  $r < r_{200}$ . The dwarf galaxy sample was constructed by selecting the galaxies with absolute magnitudes between  $-17.5 < M_V < -13$ . We analyzed the radial dependence for two distinct populations of dwarfs: galaxies which clearly show star formation activities (blue, with  $V - I < 0.95$ , and galaxies which do not have or have little star formation activity (red, with  $V - I > 0.95$ ). Fig. 13 shows the fraction of red and blue dwarf galaxies as a function of normalized radius  $r/r_{200}$ . The fraction of red dwarf galaxies (early-type) decreases toward the outskirts of the groups, while blue, star forming, dwarf galaxies (late-types) prefer to avoid the central regions of the groups. The same relation is seen in denser environments (e.g. Virgo; Sabatini et al. 2005). In their analysis of the properties of galaxy groups in the SDSS, Weinmann et al. (2006) found a similar trend for low mass systems. The fraction of early-type (red) low mass (dwarf) systems decreases with the increasing distance

from the group’s center, while the fraction of the late-type (blue) low mass (dwarf) systems increases. The fact that the dwarf galaxies in groups follow the same “morphology-radius” (“morphology-density”) relation as their bright counterparts, could be an important clue to our understanding of galaxy formation and evolution of low-mass systems.

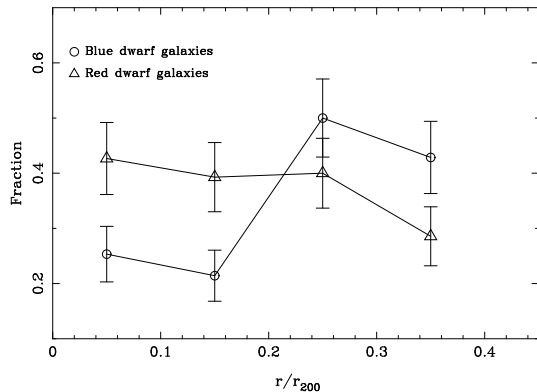


FIG. 13.— Morphological-radius relation for blue ( $V - I < 0.95$ , open circles) and red ( $V - I > 0.95$ , open triangles) dwarf galaxies with  $-17.5 < M_V < -13$ . The bars denotes Poissonian errors.

#### 6.4. Newly discovered background structures

The histograms in Fig. 9 suggest the existence of several background structures along the group line-of-sights. We used the galaxy positions and redshifts to identify the background structures in the direction of the groups.

The velocity distribution of galaxies in the background of HCG 42 group shows two significant structures at  $z \sim 0.18$  and at  $z \sim 0.25$ . The first structure (HCG42-B1), with  $RA \sim 10^h 00.2^m$  and  $DEC \sim -19^\circ 36'$ , has an elongated distribution in the N-S and E-W directions. The second structure (HCG42-B2), at  $RA \sim 10^h 00.2^m$  and  $DEC \sim -19^\circ 39'$ , is elongated in the E-W direction and more concentrated in declination. The average velocity and the velocity dispersion of these two structures are included in Table 6. The most massive structure, HCG42-B1, has 26 member galaxies. The derived velocity dispersion of  $853 \text{ km s}^{-1}$  suggest that this is a moderately rich cluster of galaxies. The second structure, HCG42-B2 with 16 galaxies, has a lower velocity dispersion ( $311 \text{ km s}^{-1}$ ), which is typical of a group of galaxies. Using the average clusters redshifts, we derived a distance of  $727 \text{ h}^{-1} \text{ Mpc}$  ( $(m - M) = 39.3$ ) and  $972 \text{ Mpc h}^{-1}$  ( $(m - M) = 39.3$ ) for HCG42-B1 and HCG42-B2 respectively. The brightest galaxy in HCG42-B1 has an absolute magnitude of  $M_V = -22.5$  (the K-correction for an elliptical galaxy at redshift  $\sim 0.2$  is  $0.15 \text{ mag}$ ; Fukugita et al. 1995) similar to the values derived for a central galaxy in rich clusters, with a morphology similar to a gE/D found in the center of most rich clusters. For HCG42-B2, the brightest galaxy has an absolute magnitude of  $M_V = -21.8$ , similar to values found for the brightest galaxies in groups.

The galaxy distribution in the direction of IC 4765 shows one well defined background structure located at  $RA \sim 18^h 47.5^m$ ,  $DEC \sim -63^\circ 18'$ . The average velocity of IC4765-B1 is tabulated in Table 6. We derived a value for the velocity dispersion of  $461 \text{ km s}^{-1}$  which is typical

for a poor cluster. At the distance of the group ( $146 \text{ Mpc}$ ,  $(m - M)_V = 35.8$ ), the brightest galaxy has an absolute magnitude of  $M_V = -22.3$ , similar to the values obtained for the central galaxy in HCG42-B1 and for central galaxies in other poor clusters.

For NGC 5846 and NGC 6868 the picture is less clear. The galaxy distribution in the direction of NGC 5846 shows several small clumps. The most important one is located at  $RA \sim 15^h 06.8^m$ ,  $DEC \sim +01^\circ 38'$  with  $cz \sim 37000 \text{ km s}^{-1}$ . However, the existence of this structure as a real cluster is dubious. In the direction of NGC 6868 we identified a second structure,  $\sim 2000 \text{ km s}^{-1}$  away from the group. This second structure is located at  $cz = 4980 \text{ km s}^{-1}$  with a velocity dispersion of  $321 \text{ km s}^{-1}$ . Two of the low surface-brightness dwarf galaxies identified as background in section 5.3 belong to this group.

## 7. SUMMARY AND CONCLUSIONS

Despite the fact that the low surface-brightness dwarf galaxies detected in the central region of groups have no membership determination, we have demonstrated the success of our method in discovering a population of dwarf galaxies with low and very low surface brightnesses that seem to be physically associated to the groups (see section 6.3 and below). Using the parameters given by the exponential fit profile, we were able to characterize the properties of the low surface-brightness dwarf galaxies in groups using a uniform and well defined criteria. At the 80% completeness limit, we were able to detected eighty low surface-brightness dwarf galaxies in the  $r < 0.5 \text{ h}^{-1} \text{ Mpc}$  region of the four groups studied here. These galaxies have central surface brightnesses  $\mu_0 \lesssim 25 \text{ V mag/arcsec}^2$ , scale lengths  $h > 1.5 \text{ arcsec}$ , and absolute magnitudes  $-16.5 < M_V < -11.5$ . The surface brightnesses and scale factors of the LSB sample are similar to those seen in Local Group dwarf galaxies. Eleven of these galaxies have large sizes and very low surface-brightness. Many of the large LSB galaxies were not identified in the original images, using the selection criteria described in section 4.1, but they were detected in the images after we convolved them with an exponential profile function to search for large and diffuse objects. Some of these galaxies are similar in size and brightness to the LSB galaxies discovered in Virgo and Fornax (Impey et al. 1988; Bothun et al. 1991) and are apparently absent in the Local Group.

A possible limitation in our survey is the criteria used to select the sample of LSB galaxies. The criteria used have been optimized to search for objects that are similar in magnitudes, sizes and surface brightnesses to those dwarf galaxies present in the Local Group. Compact, high surface brightness galaxies like M32 and very compact, high surface brightness, but faint, objects like UCD galaxies discovered in Virgo (Jones et al. 2006) and Fornax clusters (Drinkwater & Gregg 1998) are virtually missing from our sample survey. UCD and M32-like galaxies are very compact and in general they are classified as stars by SExtractor. We did not detect such objects due to the limitation imposed by the seeing and by the CLASS\_STAR limit of 0.35 used to select the LSB galaxies. Except for the Local group, M32-like galaxies are very rare and are nearly absent in other environments. If these type of galaxies are present in our sample, their numbers should be very small. In the case

of UCD galaxies the situation might be different. These galaxies are not seen in the Local Group. However, as mentioned in section 6.1, a large number of these galaxies were discovered in nearby clusters. These objects are apparently absent in groups, although searches for UCD in poor environments have just started (Mieske, West & Mendes de Oliveira 2006). We cannot discard that a population of UCD galaxies could be present in our groups. This is a pending task that requires deep, high resolution observations to search for these types of objects.

Monte Carlo simulations performed to derive the completeness fractions of LSBd detection on real images were also used to estimate the photometric errors. At  $\mu_0 \sim 25.5$  mag/arcsec<sup>2</sup> (our limit in central surface brightness), the completeness in the detection is  $\sim 80\%$ , with an error in the magnitude and in the central surface brightness  $< 0.3$  mag and  $< 0.5$  V mag/arcsec<sup>2</sup> respectively. One important result given by the simulation is our ability to determine correctly the scale factors of the galaxies. The results show that the scale factors for galaxies with  $22.5 < \mu_0 < 24.5$  mag/arcsec<sup>2</sup> and  $V < 19.0$  mag are overestimated in  $\sim 30\%$ . At fainter magnitudes and central surface brightnesses (the last bins in our simulation), the overestimation is  $\sim 60\%$ . This limitation in estimating correctly the scale factor is stronger at fainter magnitudes and could affect the correct determination of the faint-end of the Galaxy Luminosity Function by adding to the sample an undesired population of background galaxies.

In clusters (e.g. Coma and Fornax) there exists a tight color-magnitude relation for the early-type galaxies that extends to the dwarf regime. We demonstrate, as far as we know for the first time, that this relation is also present in groups (see Fig. 11), extending the relation in more than 10 magnitudes (from bright early-type to faint dwarf spheroidal galaxies). We also found that the LSBd galaxies do not show a clear correlation between magnitude and surface brightness, in contrast of what is reported in other recent studies, perhaps because the apparent observed correlation seen in other environments could be produced by selection effects. As we discussed in section 6.1, extended, very low-surface brightness galaxies could be absent from most of the surveys in groups and cluster due to a limitation imposed by the sky brightness. In fact, we were able to detect a number of large very low surface-brightness galaxies only after we convolved the images with an exponential profile function that enhanced the large, low surface-brightness features in the images.

The LSBd galaxies are clearly concentrated around the brightest group members of the groups, in a scale of  $\sim 250$  h<sup>-1</sup> kpc (see Fig. 12). At larger radius, the number density is similar to the values found in our control fields. A similar correlation is seen in other low-density environments (Vader & Sandage 1991; Carrasco et al. 2001), where bright early-type galaxies are predominant. The central concentration detected suggests that these galaxies are true dwarf galaxies of the groups. The slopes obtained from the fit to the number density profile of LSBd galaxies agree with the values derived for satellites dwarfs of isolated bright galaxies (Vader & Sandage 1991; Chen et al. 2005). Furthermore, the distribution of satellites around the centers of the groups are similar in extent to that seen in some fossil groups (e.g. NGC

1132 Mulchaey & Zabludoff 1998).

Only 78 ( $\sim 19\%$ ) of the 412 galaxies with radial velocities were confirmed as members of the groups. In addition, several new background structures were identified along the line-of-sight of the groups. In the direction of HCG 42 we identified one cluster and one group of galaxies (at  $z = 0.18$  and  $z = 0.25$ ). In the direction of IC 4765 we identified one cluster ( $z \sim 0.04$ ) and towards NGC 6868, only one poor group ( $z \sim 0.016$ ) was identified.

We have attempted to measure the radial velocities of the majority of the 80 LSBd galaxies of our list, but only eleven spectra had enough S/N for a reliable determination of their radial velocities. Only five LSBd galaxies turned out to be members of the groups. Of the six background galaxies, two are in the direction of NGC 6868 group and they are genuine dwarf galaxies which belong to a background structure located only 2000 km s<sup>-1</sup> of NGC 6868. For the remaining four galaxies, two of them have colors  $V - I > 1.3$ , two are blue and all show emission lines. It is not surprising that only few galaxies of the LSBd catalog, for which we obtained spectroscopy, are members of the groups, given that  $\sim 75\%$  of our sample have morphological types dE/dSph and therefore could not be observed due to the low S/N absorption spectra they present. About 25% of the LSBd sample are dwarf galaxies that show an irregular morphology and there is indication that they are forming stars. The four background emission-lines galaxies belong to this sub-sample and they comprise only the 30% of the total population of LSBd galaxies classified as dIrr. Hence, we estimated that only a small fraction of our sample ( $\sim 10\%$  or less) could be contaminated with background galaxies.

The dwarf galaxies ( $M_V > -17.5$ ) in the groups studied follow the same morphology-radius relation seen in much denser environments (e.g. Virgo). The fraction of red ( $V - I > 0.95$ ) dwarfs (dE, dEN, dSph) decrease towards the outskirts of the groups, while the fraction of blue ( $V - I < 0.95$ ), star forming dwarfs (dIrr) increase with cluster-centric distance. The same trend is found for low-mass systems in SDSS galaxy groups analyzed by Weinmann et al. (2006).

In this work we presented a search for low surface-brightness dwarf galaxies in poor environments at distances  $> 10$  h<sup>-1</sup> Mpc. We showed here that the technique used to search for LSBd galaxies is reliable and robust if we can derive correctly all errors associated to the detection and photometry. A good knowledge of the errors and the selection effects may give us the possibility to construct a complete, well defined sample of low-luminosity, low surface-brightness galaxies beyond the Local Group, and characterize their properties and intrinsic nature which is an important clue for testing the models of galaxy formation, in particular, at low-mass levels.

We thank the anonymous referee for useful comments and suggestions. We are grateful to the Director of Las Campanas Observatory for generous allocation of telescope time. We are also grateful to the Las Campanas and Warsaw 1.3 meters telescope personal for the excellent support and guidance during the observing runs.

ERC acknowledges support for this work provided by FAPESP PhD fellowship Nr.96/04246-7, and the support of the Gemini Observatory, which is operated by the Association of Universities for Research in Astronomy, Inc., on behalf of the international Gemini partnership of Argentina, Australia, Brazil, Canada, Chile, the United Kingdom, and the United States of America. LI wishes to acknowledge the FONDAP “Center for As-

trophysics” for support. CMdO thanks the support of FAPESP through the thematic project 01/07342-7, and CNPq through the PROSUL project. This work partially benefitted from the use of the NASA/IPAC Extragalactic Database (NED), which is operated by the Jet Propulsion Laboratory, California Institute of Technology, under contract with the National Aeronautics and Space Administration.

## REFERENCES

- Abell, G. O., Corwin, H. G. & Olowin, R. P. 1989, *ApJS*, 70, 1
- Adami, C., Scheidegger, R., Ulmer, M., Durret, F., Mazure, A., West, M. J., Conselice, C. J., Gregg, M., Kasun, S., Pelló, R. & Picat, J. P. 2006, submitted to *A&A*(astro-ph/)
- Bell, M. & Whitmore, B. C. 1989, *ApJS*, 70, 139
- Beers, T. C., Flynn, K. & Gebhardt, K. 1990, *AJ*, 110, 32
- Bertin, E. & Arnouts, S., 1996, *A&AS*, 117, 393
- Beuing, J. C., Dobereiner, S., Bohringer, H. & Bender, R. 1999, *MNRAS*, 302, 209
- Bothun, G. D., Impey, C. D., Malin, D. F. & Mould, J. R. 1987, *AJ*, 94, 23
- Bothun, G. D., Impey, C. D. and Malin, D. F. 1991, *ApJ*, 376, 404
- Bremnes, T., Binggeli, B. & Prugniel, P. 1998, *A&AS*, 129, 1
- Bremnes, T., Binggeli, B. & Prugniel, P. 1999, *A&AS*, 137, 337
- Carrasco, E. R., Mendes de Oliveira, C., Infante L. & Bolte, M. 2001, *ApJ*, 121, 148
- Cardelli, J. A., Clayton, G. C. & Mathis, J. S. 1989, *ApJ*, 345, 245
- Cellone, S. A. & Buzzoni, A. 2005, *MNRAS*, 356, 41
- Chen, J., Kravtsov, A. V., Prada, F., Sheldon, E. S., Sheldon, E. S., Klypin, A. A., Blanton, M. B. & Brinkmann, J. 2005, *astro-ph/0512376*
- Cole, S. & Lacey, C. 1996, *MNRAS*, 281, 716
- Deady, J. H., Boyce, P. J., Philipps, S., Drinkwater, M. J., Karick, A., Jones, J. B., Gregg, M. D. & Smith, R. M. 2002, *MNRAS*, 336, 851
- Dalcanton, J. J., Spergel, D. N., Gunn, J. E., Schmidt, M. & Schneider, D. P. 1997, *AJ*, 114, 635
- Dressler, A. 1980, *ApJ*, 236, 351
- Drinkwater, M. J. & Gregg, M. D. 1998, *MNRAS*, 296, L15
- Drinkwater, M. J., Phillips, S., Gregg, M. D., Parker, Q. A., Smith, R. M., Davies, J. I., Jones, J. B. & Sadler, E. M. 1999, *ApJ*, 511, L97
- de Carvalho, R. R., Ribeiro, A. L. B. & Zepf, S. E. 1994, *ApJS*, 93, 47
- de Carvalho, R. R., Ribeiro, A. L. B., Capelato, H. V. & Zepf, S. E. 1997 *ApJS*, 110, 1
- Ebeling, H., Voges, W. & Böhringer, H. 1994, *ApJ*, 436, 44
- Faber, S. M., Wegner, G., Burstein, D., Davies, R. L., Dressler, A., Lynden-Bell, D. & Terlevich, R. J. 1989, *ApJS*, 69, 763
- Ferguson, H. C. & Binggeli, B. 1994, *A&A*, 6, 67
- Flint, K., Metevier, A. J., Bolte, M., Mendes de Oliveira, C. 2001, *ApJS*, 134, 53
- Fukugita, M., Shimasaku, K., & Ichikawa, T. 1995, *PASP*, 107, 945
- Garcia, A. M. 1993, *A&AS*, 100, 1
- Geller, M. J. & Huchra, J. P. 1983, *ApJS*, 52, 61
- Gunn, J. E. & Gott, J. R. III 1972, *ApJ*, 176, 1
- Hickson, P. 1982, *ApJ*, 255, 382
- Hilker, M., Infante, L., Vieira, G., Kissler-Patig, M. & Richtler, T. 1999, *A&AS*, 134, 75
- Hilker, M., Mieske, S. & Infante, L. 2003, *A&A*, 397, L9
- Impey, C., Bothun, G. & Malin, D. 1988, *ApJ*, 330, 634
- Impey, C. D. & Bothun, G. D. 1997, *ARA&A*, 35, 267
- Irwin, M. J., Davies, J. I., Disney, M. J. & Phillips, S. 1990, *MNRAS*, 245, 289
- Infante, L. & Pritchett, C. 1992, *ApJS*, 83, 237
- Infante, L., Mieske, S. & Hilker, M. 2003, *Ap&SS*, 285, 87
- Jerjen, H., Freeman, K. C. & Binggeli, B. 1998, *AJ*, 116, 2885
- Jerjen, H., Binggeli, B. & Freeman, K. C. 2000, *AJ*, 119, 593
- Jones, C. & Forman, W. 1999, *ApJ*, 511, 65
- Jones, J. B., Drinkwater, M. J., Jurek, R., Philipps, S., Gregg, M. D., Bekki, K., Couch, W. J., Karick, A., Parker, Q. A. & Smith, R. M. 2006, *AJ*, 131, 312.
- Karick, A. M., Drinkwater, M. J. & Gregg, M. D. 2003, *MNRAS*, 344, 188
- Kron, R. G. 1980, *ApJS*, 43, 305
- Kurtz, M. J., Mink, D. J., Wyatt, W. F., Fabricant, D. G., Torres, G., Kriss, G. A., & Tonry, J. L. 1992, in *Astronomical Data Analysis Software & Systems I*, D. M. Worrall, C. Biemesderfer, and J. Barnes, eds., ASP Conf. Ser. Vol. 25 (ASP, San Francisco), p. 132
- Landolt, A. U., 1992, *AJ*, 104, 340.
- Lorrimer, S. J., Frenk, C. S., Smith, R. M., White, S. D. M. & Zaritsky, D. 1994, *MNRAS*, 269, 696
- Malamuth, E. M., Kriss, G. A., Van Dyke Dixon, W., Ferguson, H. & Ritchie, C. 1992, *AJ*, 104, 495
- Mateo, M. L. 1998, *ARA&A*, 36, 435
- Mieske, S., West, M. J., & Mendes de Oliveira, C. 2006, *astro-ph/0603524*
- Mulchaey, J. S. & Zabludoff, A. I. 1998, *ApJ*, 496, 73
- Mulchaey, J. S. & Zabludoff, A. I. 1999, *ApJ*, 514, 133
- Mulchaey, J. S., Davis, D. S., Mushotzky, R. F. & Burstein, D. 2003, *ApJS*, 145, 39
- O’Neil, K., Bothun, G. D., Schomber, J., Cornell, M. E. & Impey, C. D. 1997, *AJ*, 114, 2448
- O’Neil, K., Bothun, G. D. & Schombert, J. 2000, *AJ*, 119, 136
- Phillips, S., Davies, J. I., & Disney, M. J. 1988, *MNRAS*, 233, 485
- Ponman, T. J., Bourner, P. D., Ebeling, H. & Böhringer, H. 1996, *MNRAS*, 283, 690
- Quintana, H. & Melnick, J. 1975, *PASP*, 87, 863
- Quintana, H., Carrasco, E. R. & Reisenegiger, A. 2000, *AJ*, 120, 511
- Ramella, M., Focardi, P. & Geller, M. J. 1996, *A&A*, 312, 745
- Rood, H. J. & Struble, M. F. 1994, *PASP*, 106, 413
- Sabatini, S., Davies, J., Scaramella, R., Smith, R., Baes, M., Linder, S. M., Roberts, S. & Testa, V. 2003, *MNRAS*, 341, 981
- Sabatini, S., Davies, J., van Driel, W., Baes, M., Roberts, S., Smith, R., Linder, S. & O’Neil, K. 2005, *MNRAS*, 357, 819
- Sérsic, J. L. 1974, *Astrophysics and Space Science*, 28, 365
- Schlegel, D. J., Finkbeiner, D. P. & Davis, M. 1998, *ApJ*, 500, 525
- Secker, J., Harris, W. E. & Plummer, J. D. 1997, *PASP*, 109, 1377
- Stein, P. 1996, *A&AS*, 116, 203
- Tonry, J., & Davis, M. 1979, *AJ*, 84, 1511
- Tonry, J. L., Blakeslee, J. P., Ajhar, E. A. & Dressler, A., 2000, *ApJ*, 530, 625
- Trentham, N. 1998 & Tully, R. B. 2002, *MNRAS*, 335, 712
- Trentham, N., Sampson, L. & Banerji, M. 2005, *MNRAS*, 357, 783
- Udalski, A., Kubiak, M. & Szymanski, M. 1997, *Acta Astronomica*, 47, 319
- Vader, J. P. & Sandage, A. 1991, *ApJ379*, L1
- Weinmann, S. M., van den Bosch, F. C., Yang, X. & Mo, H. J. 2006, *MNRAS*, 366, 2
- White, D. A., Jones, C. & Forman, W. 1997, *MNRAS*, 249, 419
- Zabludoff, A. I. & Mulchaey, J. S. 1998, *ApJ*, 496, 39
- Zabludoff, A. I. & Mulchaey, J. S. 2000, *ApJ*, 538, 136



TABLE 1  
GROUP PARAMETERS

Group	RA (J2000.0)	DEC (J2000.0)	D [h <sup>-1</sup> Mpc]	$\sigma_r$ [km s <sup>-1</sup> ]	$\log(L_X)$ [h <sup>-2</sup> erg s <sup>-1</sup> ]	$A_V^{(a)}$ [mag]	$A_I^{(a)}$ [mag]
HCG 42	10 00 11.4	-19 37 02	54.5	301	41.59 <sup>(1)</sup>	0.13	0.06
NGC 5846	15 06 28.5	+01 35 10	24.1	416	41.71 <sup>(1)</sup>	0.16	0.08
IC 4765	18 47 32.9	-63 18 46	60.9	620	43.20 <sup>(2)</sup>	0.31	0.15
NGC 6868	20 09 43.0	-48 17 08	32.7	238	~ 41 <sup>(3)</sup>	0.16	0.08

REFERENCES. — X-Ray luminosity from: (1) - Mulchaey et al. (2003), (2) - Jones & Forman (1999); (3) - Beuing et al. (1999)

NOTE. — Units of right ascension are hours, minutes and seconds, and units of declination are degrees, arcminutes and arcseconds.

<sup>(a)</sup>Absorption corrections determined from the reddening maps of Schlegel et al. (1998)

TABLE 2  
OBSERVING LOG

Group	Field Id	RA (J2000.0)	DEC (J2000)	Filters	Exposure V sec	Exposure I sec	Seeing V "	Seeing I "	Area <sup>(a)</sup> arcmin <sup>2</sup>
HCG 42	F01	10 00 17.5	-19 38 32	V,I	6 × 600	3 × 600	1.2	1.2	1597.32
	F02	09 59 41.0	-19 30 41	V,I	"	"	1.3	1.1	...
	F03	09 59 41.3	-19 44 51	V,I	"	"	1.2	1.1	...
	F04	10 00 41.1	-19 44 51	V,I	"	"	1.3	1.2	...
	F05	10 00 39.5	-19 30 29	V,I	"	"	1.4	1.1	...
	F06	10 00 40.9	-18 30 33	V,I	"	"	1.2	1.1	...
	F07	10 04 39.4	-19 40 18	V,I	"	"	1.3	1.2	...
	F08	09 59 56.5	-21 20 47	V,I	"	"	1.4	1.2	...
NGC 5846	F01	15 05 23.5	+01 34 32	V,I	4 × 900	3 × 600	1.3	1.2	1397.52
	F01	15 06 16.3	+01 34 55	V,I	"	"	1.3	1.3	...
	F03	15 07 08.9	+01 34 54	V,I	"	"	1.3	1.2	...
	F04	15 06 24.3	+02 26 58	V,I	"	"	1.3	1.2	...
	F05	15 07 29.0	+00 38 33	V,I	"	"	1.2	1.1	...
	F06	15 01 50.1	+01 20 48	V,I	"	"	1.2	1.1	...
	F07	15 09 50.6	+01 34 41	V,I	"	"	1.2	1.2	...
IC 4765	F01	18 47 17.1	-63 22 27	V,I	4 × 900	3 × 600	1.2	1.5	798.48
	F02	18 47 34.5	-63 09 15	V,I	"	"	1.4	1.2	...
	F03	18 45 57.9	-62 39 50	V,I	"	"	1.3	1.2	...
	F04	18 40 02.0	-63 20 11	V	4 × 900	...	1.5	1.4	...
NGC 6868	F01	20 09 48.8	-48 17 25	V,I	4 × 900	3 × 600	1.5	1.3	399.24
	F02	20 08 31.7	-48 17 25	V	4 × 900	...	1.2	1.2	...

NOTE. — Units of right ascension are hours, minutes and seconds, and units of declination are degrees, arcminutes and arcseconds.

<sup>(a)</sup>The values are the total areas observed

TABLE 3  
PHOTOMETRIC DATA AND PROFILE FIT PARAMETERS OF LSBG GALAXIES

Galaxy id.	RA [(J2000.0)]	DEC [(J2000.0)]	$V_t$ [mag]	$M_V$ [mag]	(V - I) [mag]	$D_{iso}$ ["]	$\theta_{lim}$ ["]	$\mu_0$ [mag/□"]	$h$ ["]	$r_{eff}$ ["]	$\langle\mu\rangle_{eff}$ [mag/□"]	Type
H42-f03-2397	09 59 19.8	-19 38 11	21.03	-12.64	1.38	4.5	5.5	24.2	1.9	3.2	25.3	dE/dSph
H42-f02-2153	09 59 24.1	-19 29 05	20.04	-13.63	1.19	9.4	9.9	22.5	1.6	2.7	23.6	dE/dS0?
H42-f02-2098	09 59 25.2	-19 29 55	20.17	-13.50	0.92	5.2	5.6	23.8	1.5	2.5	24.9	dS0/dIrr
H42-f02-738	09 59 25.7	-19 32 58	20.00	-13.67	0.61	5.3	5.8	23.8	1.6	2.7	24.9	dS0/dIrr
H42-f03-L01	09 59 29.2	-19 40 59	18.32	-15.35	...	8.5	8.5	25.3	9.0	15.0	26.4	dE/dSph
H42-f02-2116	09 59 29.6	-19 28 16	19.94	-13.73	0.53	7.8	8.8	23.1	1.8	3.0	24.2	dIrr
H42-f02-L01	09 59 31.0	-19 31 47	18.59	-15.08	...	14.6	14.6	23.1	3.0	4.9	24.2	dS0,N/dIrr
H42-f03-2086 <sup>(a)</sup>	09 59 32.2	-19 43 18	20.31	-13.36	1.01	8.5	8.6	23.3	1.9	3.1	24.4	dS0/dIrr
H42-f03-1513	09 59 33.0	-19 39 54	20.73	-12.94	0.94	6.8	7.7	24.0	2.3	3.8	25.1	dE/dSph
H42-f02-408	09 59 33.1	-19 35 07	19.85	-13.82	1.21	8.0	8.7	22.7	1.5	2.6	23.9	dS0/dIrr
H42-f03-1461	09 59 34.7	-19 39 51	20.53	-13.14	0.58	7.9	9.2	23.3	2.0	3.4	24.4	dIrr
H42-f03-L02	09 59 39.3	-19 38 02	19.24	-14.43	...	9.7	9.7	24.6	4.2	7.0	25.7	dE,N
H42-f02-1939 <sup>(b)</sup>	09 59 46.8	-19 27 59	18.95	-14.72	0.87	13.9	15.4	22.9	2.9	4.9	24.0	Sp
H42-f03-1819	09 59 51.9	-19 41 36	19.37	-14.30	0.86	11.7	12.6	23.5	3.0	5.0	24.6	dE/dSph
H42-f02-1972 <sup>(a)</sup>	09 59 56.6	-19 28 08	20.41	-13.26	0.96	8.0	8.9	22.9	1.6	2.8	24.0	dS0
H42-f02-1774	10 00 03.0	-19 26 58	19.29	-14.38	0.99	11.0	12.4	23.8	3.4	5.7	25.0	dE/dSph
H42-f01-L01	10 00 03.6	-19 42 20	20.10	-13.57	...	7.2	7.2	24.1	2.2	3.8	25.2	dIrr
H42-f01-1158	10 00 09.5	-19 38 32	20.57	-13.10	0.97	7.2	8.2	23.6	2.0	3.4	24.7	dE/dSph
H42-f01-2072	10 00 13.6	-19 36 42	17.49	-16.18	1.01	23.4	25.4	22.6	4.3	7.2	23.7	dE,N
H42-f05-2229	10 00 17.7	-19 28 42	21.06	-12.61	0.82	5.5	6.1	23.7	1.6	2.6	24.8	dIrr
H42-f04-2293 <sup>(a)</sup>	10 00 23.7	-19 39 20	18.06	-15.61	1.35	33.9	33.6	23.4	7.5	12.6	24.5	dS0
H42-f04-2307 <sup>(b)</sup>	10 00 23.7	-19 39 30	19.16	-14.51	1.43	12.4	13.0	22.8	2.3	3.9	23.9	Sp
H42-f01-L02	10 00 24.5	-19 42 44	20.53	-13.14	...	5.5	5.5	24.5	2.3	3.8	25.6	dE/dSph
H42-f04-1856	10 00 41.8	-19 42 21	19.67	-14.00	0.97	12.7	13.6	23.0	2.6	4.4	24.1	dS0
H42-f04-1937	10 00 45.2	-19 42 58	19.53	-14.14	0.90	9.0	9.6	22.7	1.7	2.8	23.8	dS0/dIrr
H42-f04-1618	10 00 45.3	-19 40 39	19.00	-14.67	0.89	12.2	13.4	22.8	2.4	4.0	23.9	dE,N
H42-f05-L01	10 00 45.6	-19 24 27	19.34	-14.33	...	6.8	6.8	25.1	5.1	8.5	26.2	dE/dSph
H42-f04-1064	10 00 46.3	-19 45 15	21.29	-12.38	0.16	4.6	5.5	24.6	2.4	4.1	25.7	dIrr
H42-f04-1800	10 00 53.9	-19 42 02	20.85	-12.82	0.91	7.0	8.1	23.1	1.6	2.7	24.2	dS0/dIrr
H42-f04-1063	10 00 54.5	-19 44 56	19.99	-13.68	0.83	7.4	8.2	22.9	1.6	2.6	24.0	dS0/dIrr
H42-f04-1340 <sup>(a)</sup>	10 00 58.0	-19 38 51	21.26	-12.41	1.27	5.4	6.2	24.1	2.0	3.3	25.2	dE/dSph
H42-f05-1950 <sup>(a)</sup>	10 01 00.3	-19 27 18	21.75	-11.92	1.42	4.9	5.4	23.9	1.5	2.6	25.0	dE/dSph
N5846-f01-L01	15 04 55.7	+01 33 34	17.88	-14.02	...	8.9	8.9	25.6	12.6	21.1	26.7	dE/dSph
N5846-f01-L02	15 04 55.7	+01 41 21	19.63	-12.27	...	13.7	13.7	24.9	4.0	6.7	26.0	dE/dSph
N5846-f01-L03	15 04 55.7	+01 32 47	20.17	-11.73	...	9.0	9.0	25.1	3.5	5.8	26.2	dE/dSph
N5846-f01-1819	15 05 01.0	+01 36 35	19.33	-12.57	1.00	11.9	12.7	23.0	2.4	4.1	24.1	dS0,N/dIrr
N5846-f01-1443 <sup>(b)</sup>	15 05 21.8	+01 39 04	19.11	-12.79	0.99	11.8	12.9	22.6	2.2	3.7	23.8	Sp
N5846-f01-1996 <sup>(d)</sup>	15 05 27.9	+01 35 40	20.48	-11.42	1.25	11.9	12.8	23.8	2.4	3.9	24.9	dS0,N/dIrr
N5846-f01-343 <sup>(b)</sup>	15 05 30.6	+01 30 31	18.48	-13.42	1.22	15.6	17.1	23.7	4.4	7.4	24.8	S0/Sp
N5846-f02-L01	15 05 48.5	+01 34 50	18.98	-12.92	...	11.9	11.9	24.1	3.9	6.5	25.3	dE/dSph
N5846-f02-L02	15 05 48.5	+01 28 20	20.26	-11.64	...	10.8	10.8	24.8	2.9	4.8	25.9	dE/dSph
N5846-f02-1812	15 06 33.5	+01 39 19	19.00	-12.90	0.86	11.4	12.7	23.6	3.2	5.3	24.8	dS0,N/dIrr
N5846-f03-669	15 06 59.4	+01 33 16	19.12	-12.78	0.54	17.1	18.4	23.7	4.7	7.9	24.8	dIrr/HIIreg?
N5846-f03-1821	15 07 00.9	+01 36 19	19.11	-12.79	1.28	19.2	19.6	23.4	4.4	7.3	24.5	dE
N5846-f03-1341	15 07 01.1	+01 39 38	18.88	-13.02	0.82	16.1	18.9	24.1	6.0	10.0	25.2	dE/dSph
N5846-f03-1 <sup>(d)</sup>	15 07 02.9	+01 30 49	16.88	-15.02	0.30	60.3	65.6	23.3	14.1	23.5	24.4	dIrr/HIIreg?
N5846-f03-147 <sup>(d)</sup>	15 07 05.1	+01 30 41	18.54	-13.36	0.08	26.4	29.3	23.7	7.7	12.9	24.9	dIrr/HIIreg?
N5846-f03-268	15 07 08.3	+01 30 28	19.20	-12.70	0.42	10.8	11.8	22.6	2.0	3.3	23.7	dE/HIIreg?
IC4765-f01-1220	18 46 25.1	-63 23 34	20.30	-13.61	1.32	7.7	5.7	23.1	1.8	3.0	24.3	dE/dS0/dIrr?
IC4765-f01-L01	18 46 28.3	-63 16 31	19.92	-13.99	...	6.6	6.6	22.7	1.2	2.0	23.8	dE/dSph
IC4765-f01-1894	18 46 30.2	-63 16 37	19.39	-14.52	1.15	7.9	8.2	22.5	1.5	2.5	23.6	dE,N
IC4765-f01-L03	18 46 46.1	-63 16 46	19.98	-13.93	...	6.6	6.6	23.7	1.9	3.2	24.8	dE/dSph
IC4765-f02-518	18 46 46.2	-63 13 41	19.99	-13.92	1.20	6.5	6.3	23.9	2.2	3.7	25.0	dE/dSph
IC4765-f02-L01	18 46 48.7	-63 11 12	17.22	-16.69	...	16.8	16.8	24.9	11.7	19.5	26.0	dE/dSph
IC4765-f01-1457	18 46 57.4	-63 22 31	20.17	-13.74	...	7.5	5.9	22.9	1.6	2.7	24.0	dIrr
IC4765-f01-1707	18 47 00.3	-63 20 39	19.85	-14.06	1.32	8.5	7.1	23.4	2.3	3.9	24.6	dE/dSph
IC4765-f01-L04	18 47 01.8	-63 25 03	19.09	-14.82	...	10.1	10.1	23.4	2.5	4.2	24.5	dE/dSph
IC4765-f01-L02	18 47 05.7	-63 17 07	20.25	-13.66	...	5.6	5.6	23.2	1.3	2.2	24.3	dE,N/dSph
IC4765-f02-1620	18 47 09.1	-63 03 49	19.78	-14.13	1.10	10.4	7.1	23.2	2.9	4.8	24.4	dIrr
IC4765-f02-L02	18 47 16.5	-63 15 21	20.63	-13.28	...	4.4	4.4	24.5	2.0	3.3	25.6	dE/dSph
IC4765-f01-560 <sup>(d)</sup>	18 47 21.8	-63 26 44	20.05	-13.86	1.12	7.6	6.5	23.4	2.2	3.7	24.6	dE,N/dSph
IC4765-f01-1921	18 47 25.1	-63 17 09	20.25	-13.66	1.08	6.7	5.9	23.5	1.9	3.2	24.6	dE,N/dSph
IC4765-f02-529	18 47 25.9	-63 13 42	20.41	-13.50	0.32	5.5	5.3	23.8	2.0	3.3	24.9	dIrr
IC4765-f01-1843	18 47 51.7	-63 21 45	21.06	-12.85	1.22	5.7	4.1	23.4	1.5	2.6	24.5	dS0/dIrr?
IC4765-f02-1627	18 47 54.0	-63 03 48	20.21	-13.70	1.23	7.8	5.9	23.2	1.9	3.2	24.4	dE,N?/dSph
IC4765-f02-L03	18 48 00.9	-63 15 21	21.14	-12.77	...	4.0	4.0	23.1	1.8	2.4	24.2	dE/dSph
IC4765-f01-435	18 48 08.2	-63 26 22	16.73	-17.19	0.99	11.1	11.6	22.6	3.3	4.2	23.8	dE/dSph
IC4765-f02-2297	18 48 17.2	-63 07 21	19.58	-14.33	0.68	9.5	7.6	22.9	2.1	3.6	24.0	dS0,N?/dIrr
N6868-f02-L01	20 08 03.6	-48 21 18	20.05	-12.51	...	7.2	7.2	23.7	2.0	3.3	24.8	dE/dSph
N6868-f02-1826	20 08 48.5	-48 12 13	18.84	-13.72	...	14.4	14.5	22.8	2.9	4.9	23.9	dIrr
N6868-f02-2427	20 09 06.9	-48 15 59	20.20	-12.36	...	8.3	8.7	23.4	2.3	3.8	24.5	dE/dSph
N6868-f01-309	20 09 11.4	-48 22 56	19.83	-12.73	0.92	9.2	10.4	23.4	2.4	4.1	24.5	dIrr

TABLE 3  
PHOTOMETRIC DATA AND PROFILE FIT PARAMETERS OF LSBG GALAXIES

N6868-f01-457 <sup>(c)</sup>	20 09 12.4	-48 20 41	18.07	-14.49	1.00	23.8	25.0	23.4	5.9	9.8	24.5	dS0/dIrr
N6868-f01-1688	20 09 35.7	-48 14 22	17.43	-15.13	0.55	43.2	42.5	23.3	9.7	16.2	24.4	dIrr
N6868-f01-1971	20 09 42.6	-48 15 05	19.21	-13.35	0.96	9.0	9.9	24.1	3.4	5.7	25.2	dE/dSph
N6868-f01-2402 <sup>(c)</sup>	20 09 54.1	-48 11 48	18.66	-13.90	0.67	21.6	24.7	23.2	5.4	9.0	24.3	dIrr
N6868-f01-L01	20 09 55.7	-48 17 22	17.05	-15.51	...	17.6	17.6	25.4	17.0	28.4	26.5	dE/dSph,cloud?
N6868-f01-2361	20 10 00.1	-48 16 23	20.23	-12.33	1.12	7.6	8.6	23.9	2.5	4.2	25.0	dE/dSph
N6868-f01-1135	20 10 11.9	-48 18 33	18.70	-13.86	0.28	17.8	17.6	23.0	3.5	5.9	24.1	dS0?/dIrr
N6868-f01-2303	20 10 13.1	-48 16 11	19.40	-13.16	1.16	9.2	10.6	24.2	3.9	6.5	25.3	dE/dSph

NOTE. — Units of right ascension are hours, minutes and seconds, and units of declination are degrees, arcminutes and arcseconds.

(a) Photometry contaminated by a close object (insede 2 isophotal radius)

(b) Background galaxy (confirmed by velocity measurement): Sp - spiral, S0 - S0

(c) LSBG galaxy in the background of the group NGC 6868

(d) LSBG galaxy member of the group (confirmed by velocity measurement)

TABLE 4  
GALAXY RADIAL VELOCITIES

Galaxy	RA [(J2000.0)]	DEC [(J2000.0)]	V [mag]	(V - I) [mag]	$v_r$ [km s <sup>-1</sup> ]	$\delta v$ [km s <sup>-1</sup> ]	R/#ll	F	$v_r^f$ [km s <sup>-1</sup> ]	$\delta v$ [km s <sup>-1</sup> ]	References
H42-f02-616	09 59 12.9	-19 33 48	19.47	0.89	61532	92	11	1	61532	92	
H42-f02-956	09 59 13.7	-19 31 45	19.60	1.73	92801	53	6.6	1	92801	53	
H42-f03-2406	09 59 14.9	-19 38 11	19.50	1.11	76014	73	5.4	1	76014	73	
H42-f03-1928	09 59 15.3	-19 42 06	19.24	1.01	36122	38	10	1	36122	38	
H42-f03-990	09 59 17.0	-19 45 59	18.88	1.00	52923	45	7.2	1	52923	45	
H42-f03-805	09 59 17.6	-19 46 12	16.21	1.34	19200	18	28.5	1	19200	30	
					19218	80		1			ZM00, H42-68
H42-f03-964	09 59 17.8	-19 45 16	17.85	1.10	18972	44	12.6	1	18972	44	
H42-f02-1345	09 59 18.6	-19 24 38	19.81	1.60	70304	94	4.4	1	70304	94	
H42-f02-4007	09 59 18.7	-19 28 22	14.17	1.38	3635	15	28.4	1	3634	61	
					3621	80		1			ZM00, H42-28
H42-f03-2088	09 59 19.1	-19 43 10	19.26	1.44	55954	36	10.7	1	55954	36	
H42-f02-2234	09 59 22.7	-19 30 29	20.25	2.19	134686	66	11	1	134686	66	
H42-f03-2101	09 59 22.7	-19 43 34	19.53	1.38	114587	102	3.1	1	114587	102	
H42-f02-1898	09 59 23.2	-19 27 45	19.67	1.32	56366	43	9.5	1	56366	43	
H42-f02-1806	09 59 25.8	-19 27 07	18.36	1.19	61411	47	7.4	1	61411	47	
H42-f03-1208	09 59 25.9	-19 44 23	19.17	1.54	70919	32	11.6	1	70919	32	
H42-f03-1495	09 59 26.6	-19 38 57	17.15	0.87	3399	48	8.9	1	3399	73	
					3402	80		1			ZM00, H42-85
H42-f03-1089	09 59 27.1	-19 45 16	18.69	1.63	70553	34	14.0	1	70553	34	
H42-f03-2190	09 59 28.5	-19 43 53	18.56	1.28	70664	45	6.5	1	70664	45	
H42-f02-4008	09 59 29.0	-19 29 30	12.92	1.37	3934	22	28.1	1	3937	44	
					3980	80		1			ZM00, H42-5
H42-f03-403	09 59 29.6	-19 49 12	18.89	1.07	44052	54	5.9	1	44052	54	
H42-f03-897	09 59 29.9	-19 46 24	18.29	1.15	39928	58	6.5	1	39928	58	
H42-f02-40	09 59 30.2	-19 37 17	19.68	1.18	81018	62	5.3	1	81018	62	
H42-f03-663	09 59 30.7	-19 47 46	19.03	1.62	73883	40	12.1	1	73883	40	
H42-f02-2030	09 59 31.7	-19 28 31	19.16	1.40	73390	26	15	1	73390	30	
H42-f03-783	09 59 31.7	-19 47 17	19.27	1.47	73742	89	4.2	1	73742	89	

REFERENCES. — R96 - Ramella et al. (1996); MKV92 - Malamuth et al. (1992); S96 - Stein (1996); G93 - Garcia (1993); ZM98 - Zabludoff & Mulchaey (1998); ZM00 - Zabludoff & Mulchaey (2000), dC97 - de Carvalho et al. (1997), NED - NASA/IPAC Extragalactic database (<http://nedwww.ipac.caltech.edu/>)

NOTE. — Units of right ascension are hours, minutes and seconds, and units of declination are degrees, arcminutes and arcseconds. Table 4 is published in its entirety in the electronic edition of the *Astronomical Journal*. A portion is shown here for guidance regarding its format and content.

- (a) Galaxy observed in two different masks
- (b) Background galaxy selected as LSB
- (c) LSB galaxy in the background of the group NGC 6868
- (d) LSB galaxy member of the group

TABLE 5  
LSBD SELECT GALAXIES WITH RADIAL VELOCITIES

Galaxy	RA [(J2000.0)]	DEC [(J2000.0)]	$V_t$ [mag]	(V - I) [mag]	$\mu_0$ [mag/□"]	$h$ "	$D_{iso}$ "	$v_r \pm \delta v$ [km s <sup>-1</sup> ]
H42-f02-1939	09 59 46.8	-19 27 59	18.95	0.87	22.9	2.9	14.0	79534±169
H42-f04-2307	10 00 23.7	-19 39 30	19.16	1.43	22.8	2.3	12.4	82455±94
N5846-f01-343	15 05 30.6	+01 30 31	18.48	1.22	23.7	4.4	15.6	43856±127
N5846-f01-1443	15 05 21.8	+01 39 04	19.11	0.99	22.7	2.2	11.8	18697±30
N6868-f01-457	20 09 12.4	-48 20 41	18.07	1.00	23.4	5.9	23.8	4166±74
N6868-f01-2402	20 09 54.1	-48 11 48	18.66	0.67	23.2	5.4	21.6	4891±30
N5846-f01-1996	15 05 27.9	+01 35 40	20.48	1.25	23.8	2.4	11.9	1707±73
N5846-f03-1	15 07 02.9	+01 30 49	16.88	0.30	23.3	14.1	60.3	2815±71
N5846-f03-147	15 07 05.1	+01 30 40	18.54	0.08	23.7	7.7	26.4	2047±92
IC4765-f01-560	18 47 21.8	-63 26 44	20.05	1.12	23.4	2.2	7.6	3392±99
IC4765-f01-435	18 48 08.2	-63 26 22	16.73	0.99	22.6	3.3	11.1	5198±31

TABLE 6  
GROUP DYNAMICAL PARAMETERS

Group	RA (J2000.0)	DEC (J2000.0)	$N_{tot}$	$N_{mem}$	$\langle langle v \rangle$ [km s <sup>-1</sup> ]	$\delta v$ [km s <sup>-1</sup> ]	$r_{200}$ h <sup>-1</sup> Mpc
HCG42	10 00 11.4	-19 37 02	203	19	3845±69	296 <sup>+39</sup> <sub>-64</sub>	0.67
				36 <sup>(a)</sup>	3851±51 <sup>(a)</sup>	301 <sup>+30</sup> <sub>-43</sub> <sup>(a)</sup>	
HCG42-B1	10 00 09.0	-19 35 57		26	54541±202	853 <sup>+103</sup> <sub>-159</sub>	
HCG42-B2	10 00 11.8	-19 39 10		16	72981±101	311 <sup>+42</sup> <sub>-91</sub>	
NGC5846	15 06 28.5	+01 35 10	134	16	1983±135	513 <sup>+69</sup> <sub>-121</sub>	1.18
				32 <sup>(a)</sup>	1950±75 <sup>(a)</sup>	416 <sup>+43</sup> <sub>-63</sub> <sup>(a)</sup>	
IC4765	18 47 32.9	-63 18 46	67	33	4331±131	733 <sup>+76</sup> <sub>-111</sub>	1.66
				94 <sup>(a)</sup>	4488±65 <sup>(a)</sup>	620 <sup>+40</sup> <sub>-50</sub> <sup>(a)</sup>	
IC4765-B1	18 47 29.1	-63 16 42		16	10975±125	461 <sup>+66</sup> <sub>-115</sub>	
NGC6868	20 09 22.5	-48 18 59	57	9	2807±80	217 <sup>+37</sup> <sub>-80</sub>	0.50
				19 <sup>(a)</sup>	2844±57 <sup>(a)</sup>	238 <sup>+29</sup> <sub>-49</sub> <sup>(a)</sup>	

NOTE. — Units of right ascension are hours, minutes and seconds, and units of declination are degrees, arcminutes and arcseconds. The errors are at the 68% confidence level.

<sup>(a)</sup> Results obtained using all available velocities (our+literature)